

Postprocessing classifications of agricultural areas that base on multi-temporal radar images – Investigation of the possibilities to enhance classification results

Nachprozessierung einer Klassifikation landwirtschaftlicher Flächen auf Basis multitemporaler Radarbilder – Untersuchung der Potenziale zur Ergebnisaufwertung
Bachelor-Thesis von Korinna Schmitz
Tag der Einreichung: 17. August 2016



TECHNISCHE
UNIVERSITÄT
DARMSTADT

Fachbereich 13
Institut für Geodäsie



Korinna Schmitz
Matrikelnummer: 1703623
Studiengang: B.Sc. Umweltingenieurwissenschaften

Bachelorarbeit
Thema: Nachprozessierung einer Klassifikation landwirtschaftlicher Flächen auf Basis multitemporaler RadARBilder –
Untersuchung der Potentiale zur Ergebnisaufwertung

Eingereicht: 17. August 2016

Betreuer: Dr.-Ing. Damian Bargiel
Fachgebiet Fernerkundung und Bildanalyse
Institut für Geodäsie

Referent: Prof. Dr.-Ing. Andreas Eichhorn
Fachgebiet Geodätische Messsysteme und Sensorik
Institut für Geodäsie

Fachbereich Bau- und Umweltingenieurwissenschaften
Technische Universität Darmstadt
Franziska-Braun-Str. 7
64287 Darmstadt

Abstract

Related studies about post-processing classification generally reallocate classes into the existing pool of class labels. However, agricultural areas and their land cover change rapidly over time and cannot always be held up-to-date. As a result, not all land covers on-site are included in the classification process and appear as incorrect patches of different classes in the map. To enhance the classification results of agricultural areas, we assigned a rate of uncertainty to each pixel within a co-occurrence analysis that described the likelihood of a pixel to belong to a wrong class. Our results show that 42% to 45% of the agricultural areas lacked certainty concerning their class allocation. These areas included crops that were not considered within the set of class labels as well as vegetation-free land. The exclusion of these misclassified pixels improved the cultivation statistics. Thus, locating areas with a high rate of uncertainty substantially increases the accuracy of the classification results. It further adds to the completeness of the classification. The findings imply that conventional accuracy calculations cannot provide a clear picture of the situation on-site.



Danksagung

Ich widme diese Arbeit meiner Mutter, die stets hinter mir steht und mich dazu motiviert, das zu tun, was ich gerne mache. Sie hat mir beigebracht, dass alles möglich ist, wenn man nur will.

Weiter widme ich diese Arbeit meinem Vater, der vor vielen Jahren von uns gegangen ist, aber ohne den ich heute nicht hier wäre.

Ich möchte ein riesiges Dankeschön an meinen Freund Umar loswerden, der viel zu oft auf seine Gute-Nacht-Zeit verzichten musste, weil ich noch an meiner Thesis arbeiten wollte. Ich bin dir unendlich dankbar dafür, dass du so rücksichtsvoll und einfühlsam bist. Ohne dich wäre mein Englisch nie so gut gewesen, dass ich eine Thesis auf Englisch verfassen könnte.

Ein weiterer Dank gilt meinem ehemaligen Mitbewohner Alex, der mich dazu ermuntert hat, diese Thesis auf Englisch zu verfassen und hinterher mit der Korrektur das Nachsehen hatte. Danke, dass du trotz meiner gelegentlichen Fauxpas nicht deine Geduld verloren hat. Danke auch für das leckere Essen während meiner harten, urlaubslosen Zeit.

Als nächstes möchte ich mich sehr herzlich bei meinem Betreuer Damian bedanken, der mich stets motiviert hat, der sein Wissen mit mir geteilt hat, mir mit Rat und Tat zur Seite stand und den ich selbst in seinem Urlaub kontaktieren durfte. Ich hätte mir keine bessere Betreuung wünschen können.

Außerdem möchte ich Pouya Danke sagen, der sich im PC-Pool immer Zeit für mich genommen hat und mir mit Rat und Tat zur Seite stand.

Nicht zuletzt ein großer Dank an all meine Freunde, mit denen ich nicht immer so viel Zeit verbringen konnte, wie ich es wollte. Danke, dass ihr so geduldig ward!



Table of Contents

List of Abbreviations	vii
List of Figures	ix
List of Tables	x
1. Introduction	1
2. Background	7
2.1. Definitions	7
2.2. Initial situation	7
2.3. Classification	8
2.4. Determining the classification accuracy	9
2.4.1. Error matrix	9
2.4.2. Overall accuracy	10
2.4.3. Kappa	12
3. Methodology	17
3.1. Generalising the covered classes	17
3.2. Calculating uncertainties	18
3.2.1. Texture analysis with co-occurrence matrices	18
3.2.2. CPP approach for co-occurrence matrices	20
3.3. Smoothening the results	20
3.3.1. Image threshold	21
3.3.2. Majority filter	21
3.4. Practical realisation	21
3.4.1. RStudio	22
3.4.2. QGIS	23
3.4.3. GeoSetter	24
3.4.4. Google Earth	24
4. Results	27
4.1. Main findings	27

4.2. Texture analysis	27
4.2.1. Different textures	28
4.2.2. Varying window sizes	30
4.2.3. Iterations	31
4.3. Smoothening the results	32
4.3.1. Binary map	32
4.3.2. Majority filter	32
4.4. Developed land-cover maps	35
4.4.1. Visual comparison	35
4.4.2. Statistical comparison	36
4.5. Samples	37
4.5.1. Unknown agricultural land covers	38
4.5.2. Non-agricultural land covers	40
5. Discussion	43
5.1. Critical review	43
5.2. Comparisons to previous studies and application	45
5.3. Limitations and errors	45
6. Conclusion and outlook	49
6.1. Conclusion	49
6.2. Recommendations for further research work	49
6.3. Applicability	51
A. Maps	59
B. Code	65
B.1. Texture analysis	65
B.2. Smoothing the result	68
B.2.1. Setting a threshold	68
B.2.2. Applying a majority filter	69
B.3. Area calculation	70

List of Abbreviations

ASM	Angular Second Moment
ATKIS	<i>Amtliches Topographisch-Kartographisches Informationssystem</i> <Ger.>, meaning a federal topographic cartographic information system
CPP	classification post-processing
GeoTIFF	geo-tagged image file format
GIS	geographic information system
GLCM	grey-level co-occurrence matrix
GPS	Global Positioning System
MRF	Markov random field
PCM	primitive co-occurrence matrix



List of Figures

1.1. Exemplary comparison of visual information content between (a) maximum-likelihood-classification and (b) majority-filtering post-classification. Extract from [44, p. 290]	5
1.2. Exemplary strawberry field in the project area. Strawberries were not considered as an own class in the classification and are thus recognisable by the pattern of different class labels within a close neighbourhood.	6
2.1. RGB image of the Fuhrberg area with training (pink) and test (yellow) samples. Image recorded with Sentinel-2A on the 5th of May, 2016. Source: Copernicus Sentinel data 2016.	14
2.2. Section of the initial land cover map around Fuhrberg with training and test areas.	15
3.1. Generating grey-level co-occurrence matrices. Adapted from [25, p. 7144] for [21, pp. 612-613]	25
3.2. Demonstration of the PCM. Adapted from [25, p. 7144] for [48, pp. 4-5]	26
4.1. Statistics on the percentage of cultivation areas in the respective classes.	28
4.2. Subset images of the texture analysis with a 3×3 window around Fuhrberg.	29
4.3. Comparison of ASM and Entropy for a 3×3 window size. Subset region around Lehrte.	30
4.4. Subset images of the ASM feature with varying window sizes around Fuhrberg.	31
4.5. Subset images of iterated ASM features around Fuhrberg.	31
4.6. Subset images with different thresholds around Fuhrberg. For raw classification see fig. 4.5.	32
4.7. Comparison of a majority filter with the initial texture analysis in a subset region around Celle. Green areas showed the desired effect, while red areas aggravated the result. (a) A 3×3 ASM, then binary values with threshold 0.9. (b) A 3×3 ASM, on it a majority filter 5×5 , then binary values with threshold 0.9. Values > 0.9 stand for a high certainty, while values < 0.9 stand for a low certainty.	33
4.8. 5×5 Majority filter applied on a binary 3×3 ASM with a threshold of 0.9. Subset region of Algermissen.	34
4.9. 3×3 majority filter after 4 iterations on a binary 3×3 ASM (threshold 0.9). Subset region of Algermissen.	35
4.10. Comparison of majority filters in a subset region around Algermissen.	35

4.11. Comparison of the original and the developed land cover maps. Black areas are areas of high uncertainty and were excluded from the classification result. Subset region around Neustadt am Rübenberge.	36
4.12. Area of the respective class in the corresponding classification.	37
4.13. Unknown agricultural class: asparagus. (a) Raw classification. (b) Uncertainty map after majority filtering. (c) GPS picture of the field taken on 27-06-2016.	38
4.14. Unknown agricultural class: onions. (a) Raw classification. (b) Uncertainty map after majority filtering. (c)-(d) GPS picture of the field taken on 22-07-2015.	39
4.15. Unknown agricultural class: strawberries. (a) Raw classification. (b) Uncertainty map after majority filtering. (c) Aerial photo of the field taken from Google Earth on 01-07-2015 where people pick strawberries. (d) GPS picture of the field taken on 26-06-2016.	39
4.16. Unknown agricultural class: bee pasture. (a) Raw classification. (b) Uncertainty map after majority filtering. (c)-(d) GPS pictures with beehives taken on 04-07-2016.	40
4.17. Unknown agricultural class: ruderal species. (a) Raw classification. (b) Uncertainty map after majority filtering. (c)-(d) GPS pictures of the field taken on 26-07-2016.	40
4.18. Unrecognised class: weedy beet. (a) Raw classification. (b) Uncertainty map after majority filtering. (c)-(d) GPS pictures of the field taken on 23-07-2015.	41
4.19. Sudden change: possible ploughing up of grassland. (a) Raw classification. (b) Uncertainty map after majority filtering. (c)-(e) Aerial photos by Google Earth taken during the vegetation period 2015.	41
4.20. Non-agricultural land: recycling of building rubble. (a) Raw classification. (b) Uncertainty map after majority filtering. (c) Aerial photo by Google Earth taken on 01-07-2015. (d) GPS picturs of the field taken on 04-07-2016.	41
 5.1. Development area in Celle. (a) Final land cover map after majority filter. (b) Picture by Google Earth taken on 01-07-2015.	44
5.2. Different forms of plot borders in the study area. Pictures by Google Earth taken on 01-07-2015.	45
5.3. Before-and-after: How plot borders run into the beet field. Field close to Wietze.	46
5.4. How small areas disappear through post-processing. Subset region around Burgdorf.	47
5.5. Undetected settlements with a relatively high occurrence of oilseed rape. (a) Raw classification. (b) Final land-cover map after ASM. (c) Final land-cover map after majority filter. (d) Picture with settlements by Google Earth taken on 01-07-2015.	47

5.6. Training sample of a beet field with high occurrence of potatoes.	48
6.1. A rapeseed field end of April in the Hannover region.	50
A.1. 3 × 3 ASM Texture with a 3 × 3 majority filter on top. A value of 0 indicates a high uncertainty, while a value around 1 indicates a high homogeneity.	60
A.2. Raw land-cover map. The 13 original classes have been reduced to 6.	61
A.3. Final land-cover map. Created from a 3 × 3 ASM with a threshold of 0.9.	62
A.4. Final land-cover map. Created from a four times iterated 3 × 3 majority filter on a 3 × 3 ASM with a threshold of 0.9.	63

List of Tables

2.1. Example of an error matrix. Adapted from [10, p. 17]	10
4.1. Overview of the reduction of pixels from the raw classification through CPP. "NA" corresponds to non-agricultural areas that were excluded from the classification beforehand.	42

1 Introduction

Challenges in agriculture

The world population is growing fast, in numbers, 2.3 billion more people are expected until the year 2050. This poses a new problem to our global community. More people have to be fed, which means more food is to be grown; more cattle are to graze on pastures, which means more animal food is to be cultivated; and more energy is to be consumed, which means more energy crops are to be planted. This has the result that the demand for agricultural goods and bioenergy will increase. Farmers around the world are now facing a new challenge, namely that they have to obtain a higher yield on fewer acres. [22, p. 1]

To resolve the problem, they have relied on fertilisers and pesticides and also cultivated less diverse crops [12, p. 36]. However, intensification and overexploitation of agricultural lands have side effects, such as soil erosion [12, p. 17] and loss of biodiversity [12, p. 40], which in long-term harm productivity. An ineffective use of nitrogen and synthetic substances does not only affect the biodiversity on-site, but also causes damages in distant regions by discharging the over-concentration through the process of a run-off flow [12, p. 40].

In addition, the agricultural production has to adapt to climate change [22]. While yields could benefit from higher temperatures and a higher CO_2 level, extreme events like droughts and floods lead to water scarcity and soil erosion, which result in poor harvests [13].

To prevent the depletion of fertile land, a more sustainable production of agricultural goods is needed [22]. This includes the use of biointensive plant protection [12, p. 39], the implementation of crop-rotation sequences [12, p. 39] as well as the perpetuation of a genetic diversity of crops [16] and of fragmented land [16] (together with field margins and hedges [12, p. 40]).

In order to ensure a sustainable production of agricultural goods, a steady monitoring of land cover is needed [18]. The European Copernicus programme, a project that provides high-resolution remote sensing data to everyone free of charge, has set precisely that as one of its goals [11]. This data is crucial in the evaluation of the current state of land quality as well as trends in the use of agricultural lands. Furthermore, the programme observes in which way the change of land use affects biodiversity and landscapes [11].

Survey of land-cover information with remote sensing

The advantages of remote sensing are as follows: accessibility even in remote areas, broad regional coverage and high repeat intervals [1]. In recent years, the quality of satellite imagery has improved considerably in terms of spatial and spectral resolution [31], as in the case of radar satellite technology [4, p. 3]. Radar waves have the benefit of operating independent of

weather conditions due to their long wavelengths. They also function independently of light conditions because they actively emit radar waves and measure the backscatter. [40] The latest radar images of this type come from Sentinel-1A, a satellite operated by the Copernicus programme. This satellite is active since 2014 and has a repeat interval of 12 days [14], which means that it provides experts with a wealth of data.

Classification of remote sensing data

The data received is used to create land-cover maps. Land-cover maps are obtained by combining individual pixels into different classes (land covers). Classification is time-consuming because it is applied to a large area. For this reason algorithms have been developed that are faster and cheaper than visual data evaluation [4, p. 3]. In this context, the measured values of the remotely sensed images are converted to thematic information of the actual usage type on the ground [4, p. 10]. The type of surface cover (a class) is allocated through pattern recognition of the back radiation of a pixel and its surrounding [4, pp. 10-11].

A lot of research has been carried out in this field over the past few decades [25, p. 7140], [43, p. 395]. Traditional techniques include the maximum-likelihood-classifier [32, p. 352] and decision trees [37]. These techniques interpret the spectral information of the image pixel-by-pixel [25, p. 7140]. However, with the generation of high-resolution imagery, modelling the earth's surface has become very complex for traditional algorithms. For this purpose, new methods had to be developed, which include the neighbourhood relations of the pixels [25, ib.], [33, p. 803]. Spatial features, such as the grey-level co-occurrence matrix (GLCM) [36, p. 1277], wavelet textures [33] and morphological profiles [17] have been introduced. Object-based image analysis (OBIA) has attracted serious attention as well [5]. The extracted spatial features are fed into the classifier additional to the satellite image as a form of pre-processing, which means it is fed prior to the classification [25, p. 7140].

Once the classification or land-cover map is created, two deficiencies crop up that limit the usefulness of the map. On the one hand, the classification contains noise which distorts the map. On the other hand, the borders of the segments are not clear which aggravates the problem of distortion (see fig. 1.1a as an example).

Post-Classification

In order to remove deficiencies caused by distortion, classification post-processing (CPP) is applied. Huang et al. was apparently the first to define the term in 2014. The authors describe it as „*a refinement of the labeling in a classified image in order to enhance its original classification accuracy*“ [25, p. 7140], meaning it can smoothen and de-noise the classification. The basic idea is that adjacent pixels are more likely to be related to each other than farther distant ones. [25]

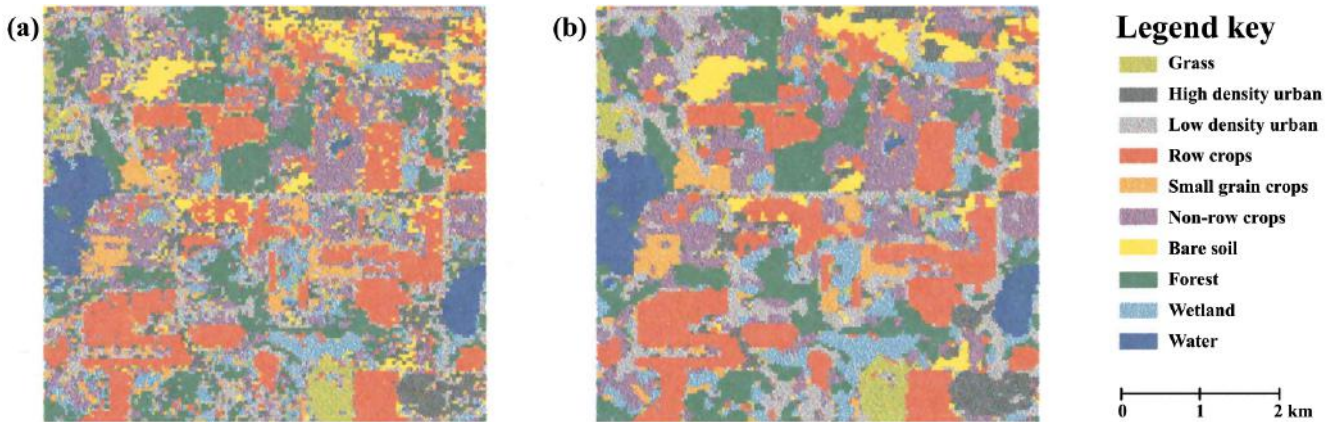


Figure 1.1.: Exemplary comparison of visual information content between (a) maximum-likelihood-classification and (b) majority-filtering post-classification. Extract from [44, p. 290]

Huang et al. [25] divided the CPP methods into four distinct categories: filtering, object-based voting, random field and relearning.

The first and simplest method is the majority filter (see fig. 1.1b) [44], which reassigned each pixel to the most common class within an $N \times N$ window surrounding the pixel [44, p. 283]. Other filters include bilateral filter [45] and anisotropic diffusion [25]. In contrast to the majority filter, these improved filters weigh the pixel in a moving window in a different way, depending on their distance and colour difference to the central pixel [25, pp. 7140-7141]. They are able to smoothen the image and at the same time preserve the edges [45].

The second method, object-based voting, divides the classification into small, uniform segments before majority voting is carried out on the borders of the segments. However, the result yields no significant improvements in the case of a pixelwise classification. [25, p. 7143]

Third is the concept of a Markov random field (MRF) [19], which assumes that every pixel has a force on the neighbouring pixels. Hence, several adjacent pixels of one class can influence an individual pixel of another class in a way that the original class of that particular pixel is moved towards the dominant class [19]. MRFs are able to smoothen and homogenise the result [25, p. 7141].

The last and latest method is called relearning and was introduced by Huang et al. in 2014. Relearning looks at both spatial arrangement and frequency of the classes and iteratively reassigned the pixels. Both types, relearning-Hist and relearning-PCM, have the functions of smoothening the classification and increasing class separability. [25]

It must be noted that even though the above described methods can achieve more precise results than the original classification (cf. fig. 1.1b), far too little attention has been paid to CPP [25, p. 7140].

Problem description

Arable lands are characterised by plots with rapid and strong changes in the spatial and temporal domain. Furthermore, there exist many different crop type classes and not all of them are necessarily considered within the training set of the classifier. This is also true for different semi-natural areas overgrown by e.g. shrubs and herbs which are also part of an agricultural landscape. These kinds of unexpected changes or classes that are not considered in the classification model produce local patches of classification errors. These errors reduce the quality of the classification result since they fill the patches with a pattern of various classes of the training set. This is also falsifying the statistics that are derived from the classification maps.

While the CPP methods as described by Huang et al. [25] can improve the classification results by giving the labels a higher probability of correctness by consideration of adjacent pixel label information and relearning, the present work is introducing a further option of CPP by assigning a rate of certainty to the defined labels. A high certainty of a class label is given when co-occurrence of similar class labels exists, whereas a high uncertainty is given when co-occurrence of different class labels exists. This definition of certainty is crucial for classifications of agricultural regions because it enables to locate areas with high error rates caused by unexpected changes or classes.

Such areas can be the ones which are planted with crops that are characterised by strong spatial and temporal variations for signal measurements (e.g. asparagus, strawberries or black currant). Further examples are special management practices conducted by farmers for certain plots but also crops that are destroyed by diseases, droughts or floods as well as abandoned land taken out of production. All these irregularly structured areas occur randomly in time and space and are usually not considered as own classes within the training data set. As a result, these areas show a pattern of different class labels within a close neighbourhood after the classification process (cf. fig. 1.2). These labels can have low or high probabilities of belonging to the classes, thus the problem of uncertainty cannot be solved by setting a probability threshold within the classification process. Accordingly, we use the measurement of the class labels' co-occurrence to define areas of high uncertainty which can be excluded from the classification map. This is not a refinement of the class labels as stated for the CPP definition of Huang et al, but it also enhances the classification accuracy in terms of giving more truth to the classification map and avoiding the inclusion of wrongly classified pixels into maps and statistics of classification products. Thus, we extend the definition of Huang et al. for CPP to: refinement and rearrangement of the labelling in a classified image in order to enhance the original accuracy, correctness and completeness of a classification result.

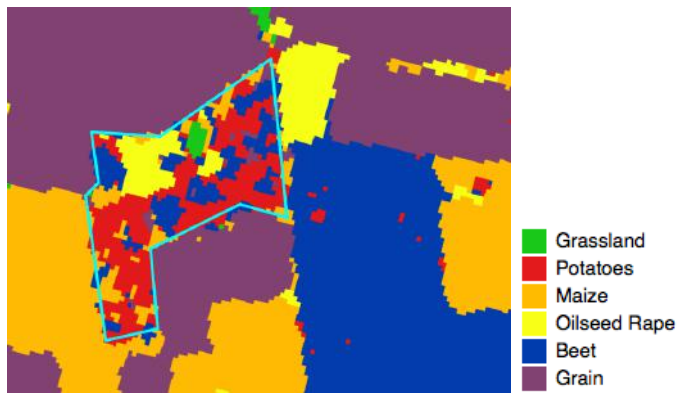


Figure 1.2.: Exemplary strawberry field in the project area. Strawberries were not considered as an own class in the classification and are thus recognisable by the pattern of different class labels within a close neighbourhood.

Objective and organisation of the study

The objective of this study is to enhance the classification results in terms of getting knowledge about areas of uncertainty.

To determine the uncertainty of areas, we used the approach of Huang et al. [25, pp. 7143-7144] to create multi-directional co-occurrence matrices in order to calculate the homogeneity of their average with the textural features suggested by Haralick et al. [21].

To the best of our knowledge, this has not been investigated so far.



2 Background

2.1 Definitions

Amtliches Topographisch-Kartographisches Informationssystem (ATKIS) is a geo-basis information system of the states of the Federal Republic of Germany. Its purpose is to acquire the topography of the German territory in a timely manner and to allocate the different object types of the ATKIS-object-type-catalogue to its areas. [3]

On one hand, **land cover** describes the physical coverage of the ground surface, including those constructed by humans. Examples are cropland (cereals, root crops, fruit trees, etc.), woodland, grassland, or artificial land. On the other hand, **land use** describes how humans are using that particular piece of land, i.e. the function of the area. Examples are agriculture, forestry, recreation, commerce or residential use. The two terms cannot always be separated from one another, so in general as well as in this study, the terms are interchangably used. [15] [39, pp. 77-78]

2.2 Initial situation

The project area is located in the North of Germany, around Hannover, the state capital of Lower Saxony. It has a size of $2,702 \text{ km}^2$. The ground is well suited for growing sugar beets and grain, such as wheat, rye and barley. Alongside, oilseed rape, maize, potatoes and asparagus are cultivated. Strawberries, carrots and lettuce can be found as well. Animal husbandry is very common too and occupies many green areas. [24], [35] An image section of the project area taken by a satellite can be seen in figure 2.1.

Data were collected using high-resolution satellite imagery from Sentinel-1A. The satellite scans the ground with a C-Band Synthetic aperture radar (SAR) with up to $5 \times 5 \text{ m}$ spatial resolution [14] at a wavelength of 5.6 m [42]. Its images are dual polarised with $VV + VH$ and $HH + HV$ (for more details see [34]).

Radar imagery has the advantage of collecting data regardless of weather conditions, i.e. its waves pass through clouds. Furthermore, it is independent of external light because it emits its own waves. [40] For this reason, there is a vast amount of data to rely on.

The classifier, whose results will be used in this study, used multi-temporal images of one vegetation period from October 2014 until October 2015. Overall, 41 time slots were observed, which amounts to 82 pictures given the fact that it dealt with 2 polarisations. It also considered



Figure 2.1.: RGB image of the Fuhrberg area with training (pink) and test (yellow) samples.
Image recorded with Sentinel-2A on the 5th of May, 2016. Source: Copernicus Sentinel data 2016.

41 images as additional features from a GLCM analysis (see section 3.2.1), which is a standard procedure in classification pre-processing [36, p. 1277].

2.3 Classification

Image classification describes the grouping of pixels into classes with the same thematic information, e.g. water, grassland, crops, etc. The result of a classification is referred to as a thematic map, or in the case of this study, a land-cover map. [43, p. 395] To distinguish between the different objects on the ground, a classification deals with the statistics of the reflected backscatter. The two common approaches are unsupervised and supervised classification. [30, p. 91]

Unsupervised classification is also known as “clustering”. With this method, pixels of the same spectral information are merged into one cluster, without knowing what this cluster represents on the ground. The user presets the number of groups, the number of iterations and a threshold. Hence, this method is suitable for areas where no information about the surface is available and shall not be further considered here. [30, p. 91]

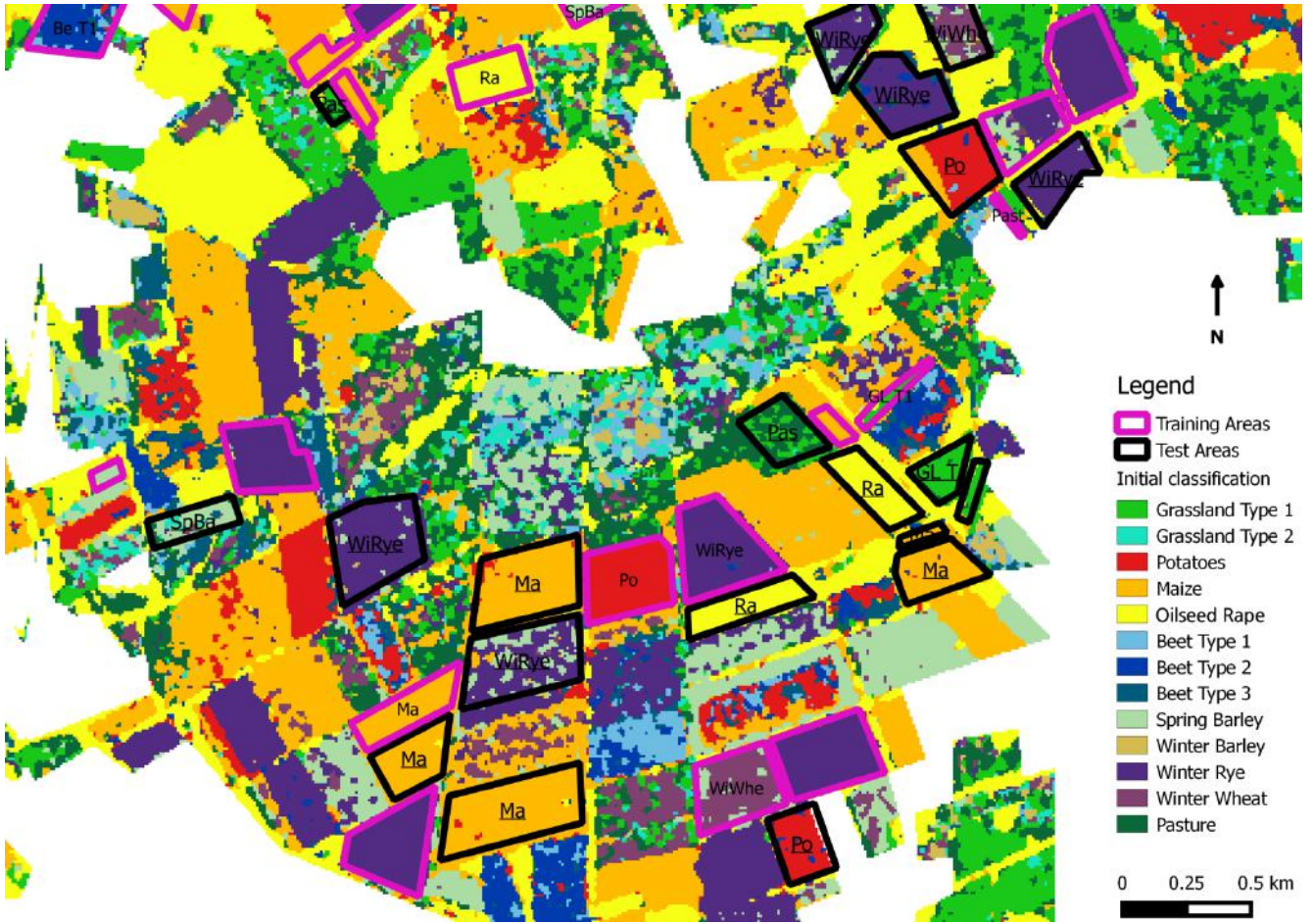


Figure 2.2.: Section of the initial land cover map around Fuhrberg with training and test areas.

Supervised classification on the other hand requires knowledge of the different ground objects in advance. This means producers have to clearly specify the desired classes beforehand and determine the class membership and location of sample areas through a field survey or other sources. Sample areas are defined as small regions of which the location and the class they contain are known. Naturally, not all areas can be taken as sample areas – otherwise there would be no need for a classification – but there have to be sufficient areas for each class to have a statistical significance. Economic constraints often limit the amount of sample areas to a minimum. The amount of recommended samples depends on the share of the respective class in the complete classification (this can be seen in detail in [46]), however, Congalton and Green suggest a minimum of 50 to 100 samples per class. According to them a random selection is equally important to avoid false values. [10]

Sample areas are divided into training and test areas. Algorithms use training areas to memorise the statistics of the pixels contained therein, or in other words, to discern how the class that is to be interpreted looks like in the spectral bands. This is possible with pattern recognition, e.g. the maximum-likelihood-classifier. [10]

Test areas or reference areas are for validation to discover how good the classifier performed. Whatever is supposed to be on the ground can be compared to the proposed class of the pixel in the same area (see section 2.4 about accuracy). Reference areas cannot simultaneously be training areas or vice versa. [10]

The result of the classification is the starting position of this study. Areas such as settlements, forests and waters have been excluded from the classification based on their entries in the ATKIS database. One pixel in the map has a resolution of $9.9 \times 10m$. An image section can be seen in figure 2.2. As a comparison, figure 2.1 shows the same section but as a true-colour satellite image before the classification. The current condition of the classification is referred to as "**initial classification**" from now on. Any advancements of this map or condition are part of this work.

2.4 Determining the classification accuracy

Specific criteria are needed to decide if a classification result is acceptable or not. Furthermore, these criteria create a standard basis for assessing, to which extent post-processing can enhance classification results. The most developed and currently most widely accepted concept for thematic accuracy is the error matrix [10], [30]. It has also been applied in the initial study (when the thematic map was created).

The following sections show how an error matrix is built and which two measures can be calculated with the help of this matrix.

2.4.1 Error matrix

$$\begin{bmatrix} C_{11} & C_{12} & \dots & C_{1k} \\ C_{21} & C_{22} & \dots & C_{2k} \\ \vdots & \vdots & \ddots & \vdots \\ C_{k1} & C_{k2} & \dots & C_{kk} \end{bmatrix}$$

A $C \times C$ error matrix (also known as confusion matrix) compares the classified data class to the reference data class for each sample [10].

- The arrangement of classes in the reference data are considered to be true. On this account, the reference data classes are referred to as validation classes [10, p. 17]. In this study, they originate from a ground survey of the reference sites.
- The classified data classes are the result of the classification process [10, p. 17]. They are subject to errors.

		Reference Data (↓)				Row sum
		W	U	AG	F	
Classified Data (↓)	W	45	0	8	12	65
	U	7	63	14	7	91
	AG	4	6	70	5	85
	F	10	3	11	66	90
Column sum		66	72	103	90	331

Land Cover Categories

W = Water

U = Urban

AG = Agriculture

F = Forest

Producer's Accuracy **User's Accuracy** **Overall Accuracy**

$W = 45/66 = 68\%$ $U = 63/72 = 88\%$ $AG = 70/103 = 68\%$ $F = 66/90 = 73\%$	$W = 45/65 = 69\%$ $U = 63/91 = 69\%$ $AG = 70/85 = 82\%$ $F = 66/90 = 73\%$	$\frac{45+63+70+66}{331} = 74\%$
--	---	----------------------------------

Table 2.1.: Example of an error matrix. Adapted from [10, p. 17]

It can be seen from table 2.1 that the classified data are normally listed in the rows ($i = \text{Rows}$), while the reference data are listed in the columns ($j = \text{Columns}$) [10, p. 60]. The values in the main diagonal, C_{ii} , represent the numbers of pixels that are assigned to the correct class i [30, p. 101]. Conversely, the values off the main diagonal, C_{ij} ($i \neq j$), represent the number of pixels that are incorrectly assigned to class i in the classification but belong to class j in reality [30]. The sum of all values in the error matrix equals the number of pixels in the classification, N (here $N = 331$) [30].

As an example, look at the first column in table 2.1. The sample areas of water include 66 pixels. 45 of those pixels are correctly classified as water. However, 7 are wrongly classified as urban, 4 as agriculture, and 10 as forest.

2.4.2 Overall accuracy

Once the error matrix is created, the thematic accuracy can be calculated. The simplest and most common statistical method is the overall accuracy [10]: the percentage of pixels that are assigned to the correct class [30, p. 101]. For this, the sum of the main diagonal is divided by the sum of all pixels:

$$\text{overall accuracy} = \frac{1}{N} \sum_{i=1}^k C_{ii}$$

In table 2.1, the overall accuracy of classification is 74%. This value is an average value and does not give any information on the extent the error is distributed among the classes. Some classes may be depicted adequately, while other classes may be more difficult to detect or to discern. [10] In dealing with this problem, there are two ways to gain knowledge about the accuracy of individual classes: the producer's accuracy and the user's accuracy.

The producer's accuracy sets out how well a certain land cover class could be identified as such by the classifier [8, pp. 36-37]. It is the ratio of correctly classified pixels in a class to the sum of column entries in that class:

$$\text{producer's accuracy } j = \frac{C_{jj}}{\sum_{i=1}^k C_{ij}}$$

By contrast, the user's accuracy aims to find out the probability that the areas indicated as class i also contain class i in reality [8, p. 37]. Here, the percentage is the correctly classified pixels in a class divided by the sum of row entries in that class:

$$\text{user's accuracy } i = \frac{C_{ii}}{\sum_{j=1}^k C_{ij}}$$

The importance of the two values can be shown with the following example. The producer's accuracy of urban areas is 88%. It would be easy to conclude that urban areas were well arranged by the classifier. However, the user's accuracy of urban areas is only 69%. This means that in 3 out of 10 times a location is stated as urban in the map but is not urban on the ground. A more conclusive analysis shows that too many pixels are listed as urban. Many belong to other classes, especially to agricultural areas. This indicates that the classifier has difficulties distinguishing among certain roof types, roads and bare soil, which favours the good result of the producer's accuracy. Consequently, it should always be looked at both values. [cf. 10, p. 59]

This problem, namely that pixels are assigned to a class they do not belong, is called a commission error. On the contrary, an omission error occurs when a pixel is missing in its rightful class. Both commission and omission errors take place simultaneously: the pixel that is misclassified is at the same time falsely counted into another class. [10]

2.4.3 Kappa

Another statistical measure of agreement is the Kappa coefficient κ , which has been introduced by Cohen [7] in 1960. The basic idea is to examine whether the correctly classified pixels in the land cover map are assigned by chance. It deducts the chance agreement (i.e. coincidental matches) from the previously calculated overall accuracy (i.e. the accordance between reference sites and land cover map). The result is a new (or different) estimate of total classification accuracy that is independent of chance:

$$\kappa = \frac{p_0 - p_c}{1 - p_c}$$

p_0 is the percentage of actual agreement, which is introduced as overall accuracy:

$$p_0 = \frac{1}{N} \sum_{i=1}^k C_{ii}$$

p_c is the percentage of coincidental matches in p_0 . Therefore, the sum of row entries is multiplied by the sum of column entries separately for each class. Then, these products are added up. To get a ratio, this value is divided by the total number of pixels, N , squared.[7] In the following, Nr_i and Nc_j are used to describe the total number of pixels in a row or column respectively.

$$p_c = \frac{1}{N^2} \sum_{i=1}^k Nr_i \cdot Nc_i$$

The Kappa analysis is a good estimate for sample sizes of a multinomial distribution [9, p. 152], [10, p. 105]. κ takes values between -1 and $+1$. A κ value of 1 only occurs if there is full agreement between the classification and the reference sites (i.e. values off the main diagonal are zero) [7]. Values ≤ 0 indicate that the elements on the main diagonal arose solely by chance [7]. Self-evidently, values of κ are either equal to or smaller than the overall accuracy.

According to Landis and Koch [28, p. 165], values greater than 0.8 are said to be excellent and values between 0.4 and 0.8 are acceptable to considerable.

In example 2.1, κ is calculated as follows:

$$p_0 = \text{overall accuracy} = \frac{45 + 63 + 70 + 66}{331} = 0.74$$

$$p_c = \frac{(66 \cdot 65) + (72 \cdot 91) + (103 \cdot 85) + (90 \cdot 90)}{(331)^2} = 0.25$$

$$\kappa = \frac{0.74 - 0.25}{1 - 0.25} = 0.65$$

0.65 means that there is a 65% better agreement than purely by chance [cf. 7]. The strength of agreement is considerable.

3 Methodology

The classification accuracy of an image cannot always be further improved. A look on figure 2.2 on page 15 reveals that the test areas themselves were identified in a sufficient way. There were rather the tessellated areas in the land-cover map that confused the user.

As it has already been pointed out in the introduction to this study, these tessellated areas arose from classification errors, e.g. because the classifier was not trained in recognising the land cover of the underlying pixels. Classes that were not part of the classification included woodlands, swamps and rarely cultivated plants. It is known e.g. that strawberries and asparagus were grown in the study region but were not considered in the set of class labels. Furthermore, not all urban areas, forests or roads were registered as such in ATKIS so that these areas erroneously were not eliminated from the classification.

The classifier was not aware of these issues and notwithstanding assigned a class to the previously stated regions. Thereby it chose the class with the highest probability based on the statistics of the pixel and its surrounding; even though the probability for that particular class might have been very low.

These areas could not be improved through conventional CPP filters, since all conventional methods merely reassign pixels to other existing classes. Instead, a new approach was needed that excluded areas from the map that seemed to contain wrong information about the situation on the ground. These areas could be detected through their lack of homogeneity. For this reason, a method is introduced that used simple spatial-dependant textural features to determine areas of high uncertainty. Subsequently, post-processing methods were applied to emphasize the result. The last part of this section focuses on the programs and functions used in this study.

3.1 Generalising the covered classes

Before proceeding to compute the uncertainties it was necessary to initiate some broader classes. The initial classification included thirteen different classes, which partly contained very similar information. When calculating these uncertainties, classes that were difficult to separate (such as rye and wheat) should not be taken into account. As mentioned before, the main focus was set on the tessellated areas of high uncertainty. Some of the classes from the initial classification therefore were subsumed under a major class. The following new classes were introduced:

- Grassland type 1 and type 2 as well as pasture were put in the new class grassland.
- Beet type 1, type 2 and type 3 were put in the new class beet.

- Spring barley, winter barley, winter rye and winter wheat were put in the new class grain.

After the reclassification, there were six classes left: grassland, potato, maize, oilseed rape, beet and grain. The simplified classification is referred to as "**raw classification**" hereinafter.

3.2 Calculating uncertainties

In a next step, regions that suffered from a lack of homogeneity should be identified through textural feature extraction. A lack of homogeneity refers to an accumulation of different classes within small distances. Textural feature extraction is a standard procedure in image classification at present [36, p. 1277]. In spite of that, it is a new method in the scope of CPP, introduced by Huang et al. in 2014 [25].

Textural features are based on GLCMs, whose creation is demonstrated first, after which the relevant features to calculate uncertainties are pointed out. In the second part, an approach for implementation in CPP is presented.

3.2.1 Texture analysis with co-occurrence matrices

Haralick et al. [21] already published a paper on "Textural Features for Image Classification" as far back as 1973. In it, the authors explain that the spatial arrangement of grey tones can provide information about the content on the ground which can be used to identify and then classify similar structures in an image. The spatial arrangement of the various shades of grey is captured in a so called grey-level co-occurrence matrix (GLCM).

A GLCM displays the frequency of transitions from pixels with grey tone i to pixels with grey tone j in a determined direction dir and distance dis . Step-by-step, a square window of size ω is slid over the image and in each step a GLCM is allocated to the respective central pixel. [21] As shown in figure 3.1, the 4×4 image is composed of grey level values from 0 to 3. The window size ω complies with the size of the image here. It is counted how many times pixels with grey tone i are the horizontal (0 degrees), vertical (90 degrees) or diagonal (45 and 135 degrees, resp.)¹ nearest ($dis = 1$) neighbours to pixels with grey tone j . The numbers are entered in the appropriate cell $\#(i, j)$. [21, p. 613]

Haralick et al. proposed fourteen textural features [21, p. 619] that can be obtained from a GLCM. In this work only four were relevant in the context of representing uncertainties:

$$\text{Angular Second Moment} = \sum_{i=0}^{N-1} \sum_{j=0}^{N-1} (p(i, j))^2 \quad (3.1)$$

¹ Note that when calculating directions, the opposite direction ($+180^\circ$) is counted as well. This explains why the values on the main diagonal in figure 3.1 are double.

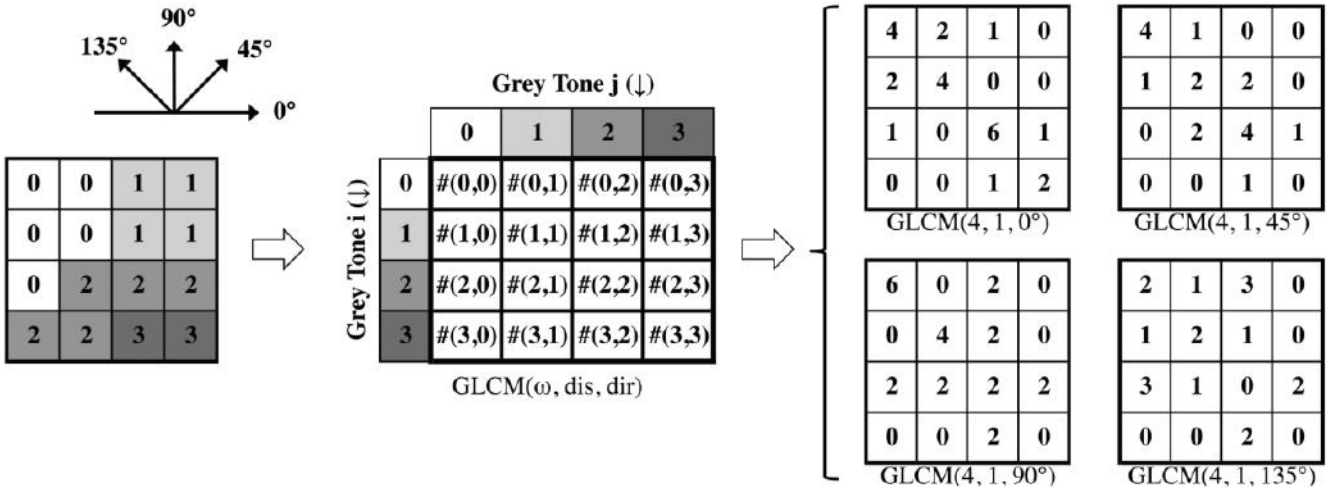


Figure 3.1.: Generating grey-level co-occurrence matrices. Adapted from [25, p. 7144] for [21, pp. 612-613]

$$\text{Variance} = \sum_{i=0}^{N-1} \sum_{j=0}^{N-1} (i - \mu)^2 \cdot p(i, j) \quad (3.2)$$

$$\text{Entropy} = - \sum_{i=0}^{N-1} \sum_{j=0}^{N-1} p(i, j) \cdot \log(p(i, j)) \quad (3.3)$$

$$\text{Homogeneity} = \sum_{i=0}^{N-1} \sum_{j=0}^{N-1} \frac{1}{1 + (i - j)^2} \cdot p(i, j) \quad (3.4)$$

where N corresponds to the range of grey levels in a quantized image; i and j represent the different grey tones in the window; $p(i, j)$ constitute the normalised frequencies for the neighbourhood of grey tone i and j in the respective dir and dis in the window; and μ is the mean. Those features are calculated for each window and its value is allocated to the central pixel. Per direction, distance and window size, a new structural image arises.

The *Angular Second Moment (ASM)* measures the similarity of an image and the distribution of entries in the GLCM. It ranges from 0 to 1. The value is close to 1 when there are few but large entries in the matrix. This is the case when values in the matrix have very similar shades of grey, or when they consistently alternate between the same grey tones i and j . [36, p. 1283]

The *Variance* is not dependant on the co-occurrence of pixels. It describes the grey-level variance in the specific window. Its value is high when the standard deviation of the grey levels in the window is high. [36, p. 1283]

The *Entropy* describes the disorder in an image. It is zero when all grey levels are the same (homogeneous). By contrast, it is high when many different grey levels are located in the window. [36, p. 1283]

The *Homogeneity*, or the *Inverse Difference Moment* [21, p. 619], specifies if similar grey tones in the image are in immediate vicinity. It depends on the distance of grey-scale values within the window. Small differences in grey tones result in high values. The *Homogeneity* can assume values from 0 to 1, where 1 refers to a homogeneous image. [36, p. 1282]

In addition, Haralick et al. suggests to combine GLCMs of different directions but same distance in a multi-directional GLCM and to use their mean and range for the proceeding classification. Consider two identical images but one turned by 90 degrees. The textural features will have the same values but in a different order, so that it appears that the images are not the same. By calculating the average of all the directions, the two images will be found to correspond. [21, p. 615]

3.2.2 CPP approach for co-occurrence matrices

In 2014, Huang et al. [25, pp. 7143-7144] took Haralick's approach and applied it as a CPP method. To do so, the authors replaced the grey level values from the previous subsection with the different class numbers of the classification. Associated therewith, the term GLCM was renamed to primitive co-occurrence matrix (PCM). In this study, the idea of PCMs was adopted to assess the lack of certainty among the classes.

The PCMs were calculated in the following way (see figure 3.2) [adapted from 25]. At first, the classification was divided into C different classes. Then, for each pixel, PCMs of the size $C \times C$ were generated², where $\#(C_i, C_j)$ indicated the number of times a certain transition from one class to another in direction dir and for a window size ω had been registered. These were written down as $PCM(\omega, dis, dir)$. The regarded directions were 0 degrees, 45 degrees, 90 degrees and 135 degrees. To minimise the computational burden, the distance dis was set to 1 for all matrices. Certainly, further offsets could have increased the information content but they complicated the problem at the same time and are not discussed at this point.

The next step was to calculate relevant textures individually for each PCM with the aforementioned equations 3.1 - 3.4. After that, the different texture values of the same pixel were averaged. As said before the distance dis had been set to 1, so that an direction-independent texture remained, which solely depended on ω . The window size ω consecutively was set to 3, 5, 7 and 9.

² In case of 6 classes, the PCM will hence be a 6×6 matrix.

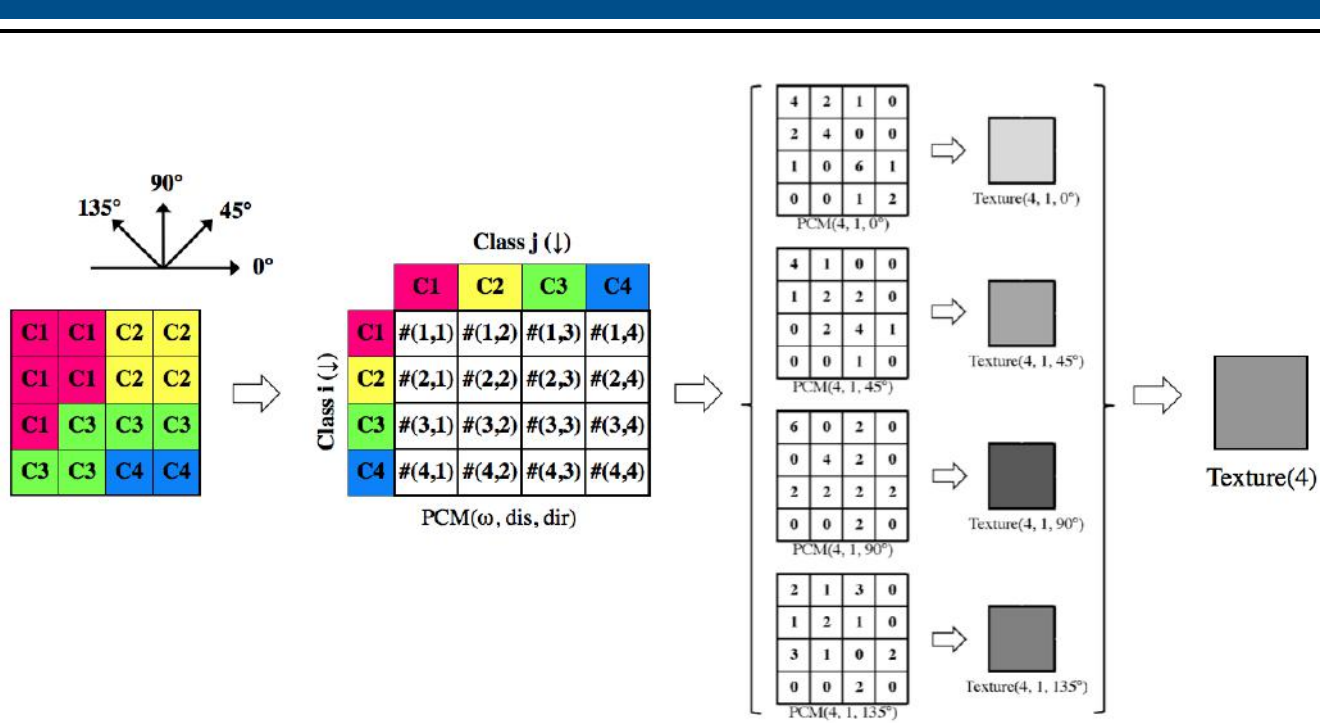


Figure 3.2.: Demonstration of the PCM. Adapted from [25, p. 7144] for [48, pp. 4-5]

$$\text{Texture}(\omega) = \sum_{dir} \text{Texture}(\omega, dis, dir) , \quad \text{for } dir = [0^\circ, 45^\circ, 90^\circ, 135^\circ] \quad \text{and} \quad dis = 1.$$

The idea behind this approach was very simple: if an area in the classification was homogeneous, i.e. most of the values in the PCM were on the main diagonal, they would still be located there after all values had been averaged. By contrast, if an area was rather heterogeneous, i.e. the values in the PCM were distributed over the entire matrix and less values were on the main diagonal, the probabilities to the square in equation 3.1 (the certainty) would decrease more as the initial values disperse.

The values of the texture calculations were entered in a new map, the **uncertainty map** (see code in Annex B.1). Regions that were likely to be classified incorrectly stood out by their colour.

3.3 Smoothening the results

In the last section, it has been explained how the uncertainty map was created. The part that follows moved on to consider how these results could be improved with conventional image processing tools. In particular, it was to be investigated how to make a clearer distinction between areas of uncertainty and areas of certainty.

The uncertainty map of section 3.2.2 was made out of a range of values that showed the probability of a particular pixel belonging to the right class. One marginal value stated that the class allocation was accurate, while the other stated a high unlikelihood. Regions in which a

high uncertainty prevailed should be highlighted. To achieve this, two methods were applied: the first one separated certain and uncertain regions, the other one smoothed the result.

3.3.1 Image threshold

First, the contrast between uncertain and certain areas should be maximised. For this purpose a black-and-white image, a so called binary image, was created.

Let us suppose the newly obtained uncertainty map U had k grey level values $0, 1, 2, \dots, k - 1$. A threshold value T was defined within the range of grey levels $T \in \{0, 1, 2, \dots, k - 1\}$ to which the grey tone of every pixel was compared and assigned to either 0 or 1. [6, p. 71] According to the decision criterion, the new binary image was created in the following way:

$$B(n) := \begin{cases} 0 & \text{if } U(n) \leq T \\ 1 & \text{if } U(n) > T \end{cases} \quad \text{for every cell } n \text{ in } U$$

where $B(n)$ represents the value of pixel n in the binary map, and $U(n)$ stands for the grey level value of pixel n in the uncertainty map [6, p. 71]. See code in Annex B.2.1.

3.3.2 Majority filter

After the binary map had been obtained, the next method aimed at smoothing the result and at accumulating regions of high uncertainty. This step involved the majority filter.

Majority filtering is a standard method in CPP. The filter assigned the most frequent class inside a window of size ω to the central pixel. [44, p. 283] See the code in Annex B.2.2 for more details. On the one hand, the filter had the task to remove isolated black or white points from the map, which might confuse the user. On the other hand, it should merge areas of mixed pixel values into a big area of the more predominant value (certain or uncertain).

3.4 Practical realisation

3.4.1 RStudio

We decided that the best program to manipulate a grid and to calculate textural features in this investigation was RStudio. RStudio is an integrated development environment for the programming language R which is gaining popularity among users worldwide [47]. R is a procedural language which is used for statistical computing and graphics. It is applied in the economic as well as in the academic world.

RStudio is open-source and can be executed on any platform, such as Windows, Mac and Linux. Moreover, it cannot only be accessed on desktop but also in a web browser. The code is written and stored in scripts. Storing the code in scripts has the advantage that the results are transparent and reproducible. Apart from that, each command is stored in the history tool and can be retrieved later.

Predefined commands on various issues can be obtained in the form of packages. Packages include several functions or automated tasks. Users can contribute by developing their own functions or modifying the functions of others. As previously mentioned, the R community is growing, so that there are currently over 8000 packages available in the CRAN (Comprehensive R Archive Network) repository. The packages used in this investigation are explained in the following sub-chapters.

The principal arguments for RStudio are the following three. First, the program environment and the packages are free of cost, whereas MATLAB and its toolboxes (e.g. the Image Processing Toolbox) are costly. Second, RStudio has a great variety of packages especially in the field of remote sensing, addressing raster, classification or feature extraction. Third, the R community has presented itself actively and helpfully online, so that solutions to various problems can be found in forums.

"sp" package

The package "sp" from Pebesma and Bivand [38], version 1.2-3, provides various classes and functions for spatial data. The classes record for example where the spatial information of an object is written. The function "stack" saves the different textural features for one particular window size in an eponymous stack.

"raster" package

The "raster" package from Hijmans [23], version 2.5-2, offers functions to read, analyse, manipulate and save gridded spatial data. It was used among others to create a raster layer from the initial classification. Once all calculations were done, the resulting textural features were written into an image in geo-tagged image file format (GeoTIFF). GeoTIFF has been chosen because the format enables a lossless storage and delivers an optimum image precision.

Furthermore, some classes of the initial classification were subsumed under a superordinate new class to measure uncertainties in the classification only between species that are not related. The reason for the rearrangement was to detect tessellated areas where the classifier could not decide on one class, e.g. because it did not recognise this particular land cover. For this task the function "reclassify" was used.

The same function was used to create the binary map as well. Values lower or equal to the threshold value T were assigned to 0, the remaining values were assigned to 1.

Subsequently, the functions "focal" and "modal" were used to find the predominant value in a neighbourhood. "Focal" forms a window area around the pixel of reference, while "modal" finds the most frequently occurring number in each position.

"glcm" package

The "glcm" package from Zvoleff, version 1.6.1, has been used to calculate image textures of a classification with the help of GLCMs. The function of the same name, "glcm", defines consecutively co-occurrence matrices and textural features. First, GLCMs are created in each moving window of size ω for a given distance dis and direction dir . Following the example of Huang et al. [25, pp. 7143-7144] matrices were generated over shifts of four different directions (namely 0 degrees, 45 degrees, 90 degrees and 135 degrees) for a constant distance $dis = 1$ (see chapter 3.2.2). The texture was calculated individually for each direction and the values in the cells were then averaged over all directions. Pixels without values (e.g. gaps in the classification in residential areas) were ignored in the creation of GLCMs. [48]

In the framework of the study, homogeneity, angular second moment, entropy and variance have been of particular interest. The equations used in the function originate from Haralick [21, p. 619] and accord with the equations 3.1 - 3.4.

3.4.2 QGIS

QGIS, formerly Quantum-GIS, is an open-source geographic information system (GIS) application to view, analyse and edit spatial data. The main features of the application in the framework of this investigation are the support of many frequent vector and raster data, such as "shapefile" and GeoTIFF, and the creation of maps. The program has been particularly useful in displaying GeoTIFFs because the files were too big for a regular picture viewer. It was preferred to ArcGIS because it is free of charge. In this way, usage on personal computers was made possible.

3.4.3 GeoSetter

GeoSetter [41], version 3.4.16, is a free software to save and display geographic coordinates in image files. For this, it includes a background map from Google Maps. It has been used in the study to identify the exact position and shooting direction from which the pictures were taken with the camera on-site.

3.4.4 Google Earth

Google Earth [20], version 8.0.3.2344, is a free software of the company Google Inc., which displays satellite imagery, aerial and ground photographs in different resolutions and superimposes them with geographical data. Its advantage over Google Maps is that it shows the recording date of the image and even more importantly shows a time axis of different pictures taken at different times. In this way, it was possible to retrospect and verify the land cover of the fields in 2015.



4 Results

4.1 Main findings

Layer	Area in km ²						Classes sum	Unclassified	NA	Total
	Grassland	Potatoes	Maize	Rape	Beet	Grain				
Raw classification	235	60	200	330	130	511	1.467	0	1.234	2.702
After ASM	130	14	94	164	69	373	845	621	1.235	2.702
After majority filtering	123	12	89	151	66	366	807	655	1.239	2.702

Table 4.1.: Overview of the reduction of pixels from the raw classification through CPP. "NA" corresponds to non-agricultural areas that were excluded from the classification beforehand.

Two land-cover maps were created by means of a co-occurrence analysis and an additional filter (fig. A.3 and A.4, respectively), which demonstrated the inconsistencies in the classification graphically. The study showed that a co-occurrence analysis markedly improved the quality of an agrarian classification result. Only 845 km² or 807 km² out of 1,467 km² of the allegedly known agricultural land was certain to belong to one of the predefined classes after a 3 × 3 ASM calculation and a following 3 × 3 majority filter, respectively (table 4.1). This means that 42 (after ASM) or 45 (after majority filtering) out of 100 agriculturally used pixels were subject to uncertainty concerning their class allocation and should be revised or excluded from the map. To validate the plausibility of the questioned areas, random samples that showed a high level of uncertainty were taken and their land cover examined on-site. It was found that the co-occurrence analysis detected areas where plants such as asparagus, onions or ruderal species were growing (see chapter 4.5). Vegetation-free land, such as settlements and barren land, was identified as well.

The developed map therefore enhanced the classification results in a way that it increased the accuracy without the traditional reallocation of pixels. By blackening patches with mosaic-like arranged classes (uncertain areas) of the original classification, the visual appearance for the user improved. Conspicuous areas used to attract higher attention than single-coloured fields. In its current state, the actual field-covers were much clearer to recognise (fig. A.4).

Moreover, the inclusion of falsely classified pixels into the initial map led to false statistics of farmland. After the statistics had been upgraded with the data of the developed classification map, the share of grain interestingly increased by 10% (fig. 4.1). Oilseed rape reduced its appearance by 4%.

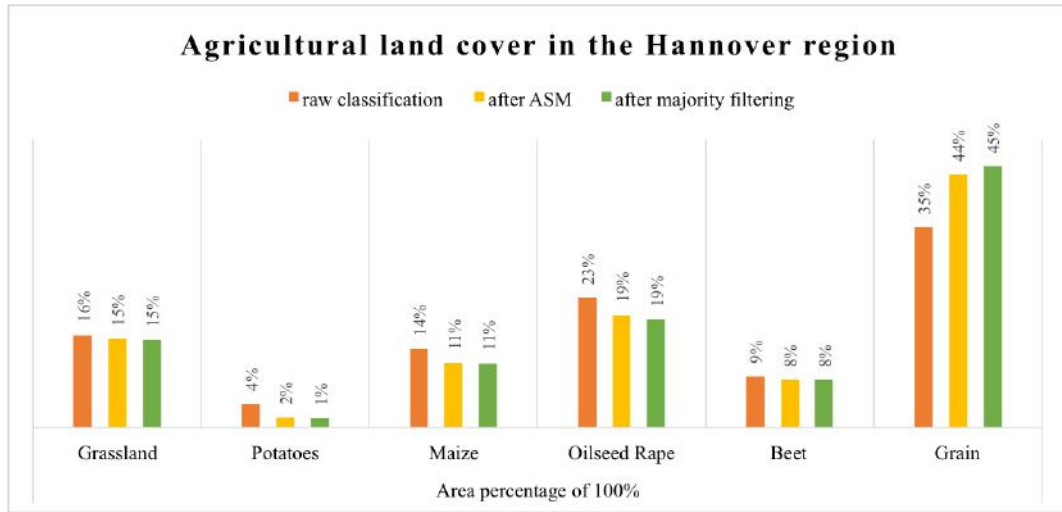


Figure 4.1.: Statistics on the percentage of cultivation areas in the respective classes.

4.2 Texture analysis

Simple statistical texture analysis was used to determine wrongly classified pixels in a neighbourhood. For this, four textural features were chosen beforehand: *ASM*, *Variance*, *Entropy* and *Homogeneity* (see chapter 3.2.1). With varying experiments, the version with the best ratio between broad field coverage and narrow field borders was sought. The distance of the pixels was set to 1. The textures were averaged over all directions (0° , 45° , 90° , 135°).

4.2.1 Different textures

Note that in this section the classification still consisted of thirteen classes. Behind the classification stood a matrix where each class was represented by a number between 1 and 13.

First, the textures were calculated with a window size of 3×3 pixels.

The *Homogeneity* map had bright regions, which stood for a low uncertainty, and dark regions, which stood for high uncertainty (fig. 4.2e). Although the visual appearance of the layer looked appealing at first sight, the main drawback was that the feature included the distance of the class numbers in its calculation (see equation 3.4). That is why in figure 4.2e some inhomogeneous areas seemed darker than others. Potatoes (class number 3) and maize (class number 4) for example showed brighter results when next to each other than grassland (class number 1) and pasture (class number 13). However, both results should show the same shades of grey because in both cases the classifier could not assign a class with clarity.

The *Variance* map (fig. 4.2f) faced a similar problem as the *Homogeneity* map. Regions with a low class number seemed darker on the map (e.g. maize with class number 3), while regions with a high class number were brighter (e.g. winter rye with class number 11). This means that

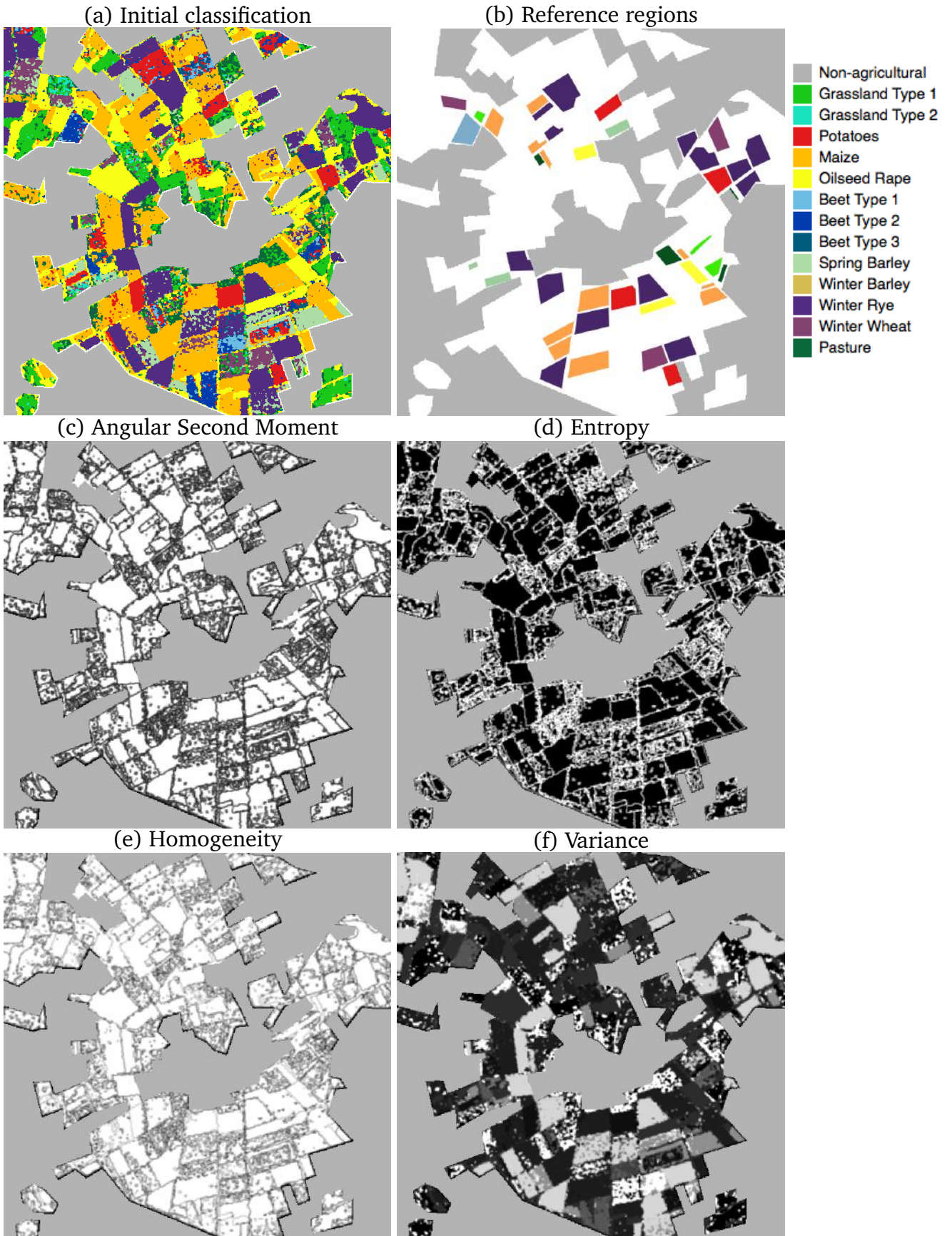


Figure 4.2.: Subset images of the texture analysis with a 3×3 window around Fuhrberg.

both dark and bright colours could be homogeneous or diverse, so that the same problem arose as in the initial situation of this study. As explained in [2, p. 6], the function emphasizes values that diverge from the mean value of $p(i, j)$ (see equation 3.2).

Entropy and *ASM* looked very similar (fig. 4.3). However, *Entropy* has high values when the regions are homogeneous (fig. 4.2d), whereas *ASM* has high values when the regions are inhomogeneous (fig. 4.2c). Both textures presented satisfactory results.

Figure 4.3 illustrates that in both cases, homogeneous areas in the classification were left blank in the texture analysis. Inhomogeneous regions were visible as black pixels. The degree of blackness determined the degree of uncertainty towards the picture allocation. Field borders, although not necessarily inhomogeneous, were detected as well (see section 5.3). *ASM* was chosen for the further course of the investigation.



Figure 4.3.: Comparison of *ASM* and *Entropy* for a 3×3 window size. Subset region around Lehrte.

4.2.2 Varying window sizes

The 3×3 *ASM* feature is characterised by line-type structures. The objective of this study, however, was to find inhomogeneous surfaces that cover large areas. For that purpose, it was examined whether these structures can be extended by larger window sizes. In the following, window sizes of 3, 5, 7, and 9 are compared.

Figure 4.4 shows how the dark lines merged with one another as expected, but at the same time filled the homogeneous areas. Overall, the goal was not reached.

4.2.3 Iterations

Since bigger window sizes were unsuccessful but the aim remained to create broader inhomogeneous regions, iterations of the *ASM* feature were performed. This means that an *ASM*

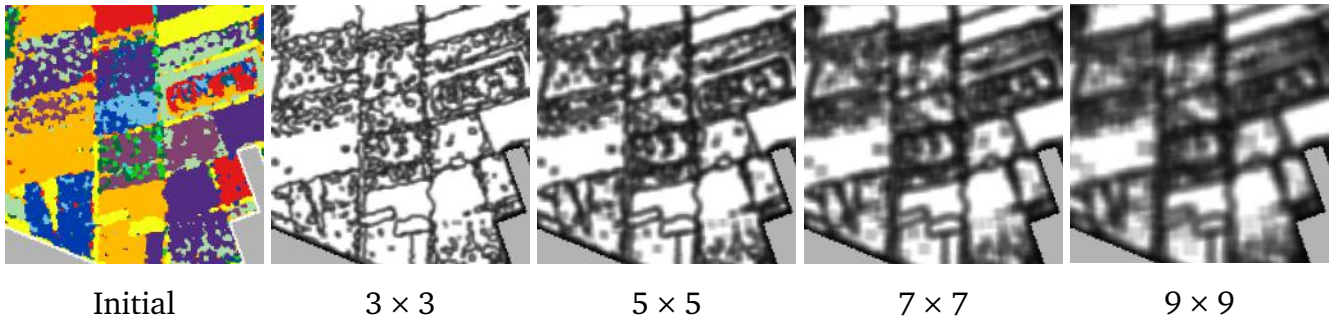


Figure 4.4.: Subset images of the ASM feature with varying window sizes around Fuhrberg.

textural analysis was applied to the former result of an *ASM* textural analysis. For this, the map containing the textures was discretised to 13 values to keep the computation power down¹. Note that the map contained only six classes from this point on (cf. section 3.1). In this way, pixels were prevented from being detected as uncertain solely because they were confused with another class from the existing set of class labels due to similar spectral information, as it was the case for different types of grassland.

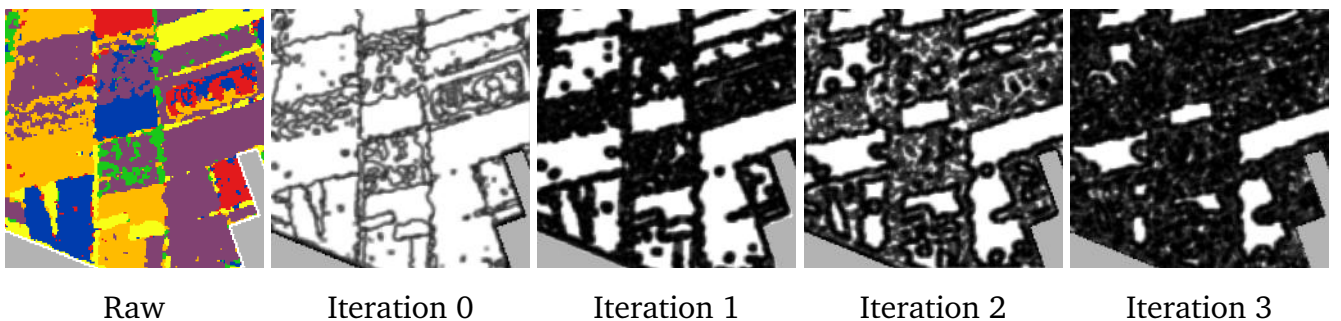


Figure 4.5.: Subset images of iterated ASM features around Fuhrberg.

As shown in figure 4.5, the inhomogeneous regions spread rapidly across actual homogeneous regions and took up too much space. Thus, the iterations did not have the desired effect. In conclusion, a 3×3 ASM feature without iteration led to the best results.

4.3 Smoothening the results

While the last section focused on improving the uncertainty map with textural features, the next section of the study was concerned with the improvement of the developed uncertainty map with conventional image-processing tools. The purpose remained to transfer the inhomogeneous lines into an inhomogeneous surface.

¹ Note that a PCM has to be created for every moving window, so for many decimal numbers the co-occurrence matrix increases exponentially.

4.3.1 Binary map

To make a clearer distinction between certain and uncertain regions, the uncertainty map was first converted into a binary image (cf. section 3.3.1). In this way, dark (inhomogeneous) pixels are emphasized. The current 3×3 ASM uncertainty map had values from 0 to 1, which corresponded to a high uncertainty and a low uncertainty respectively. Thresholds of 0.6, 0.7, 0.8 and 0.9 were set and compared.

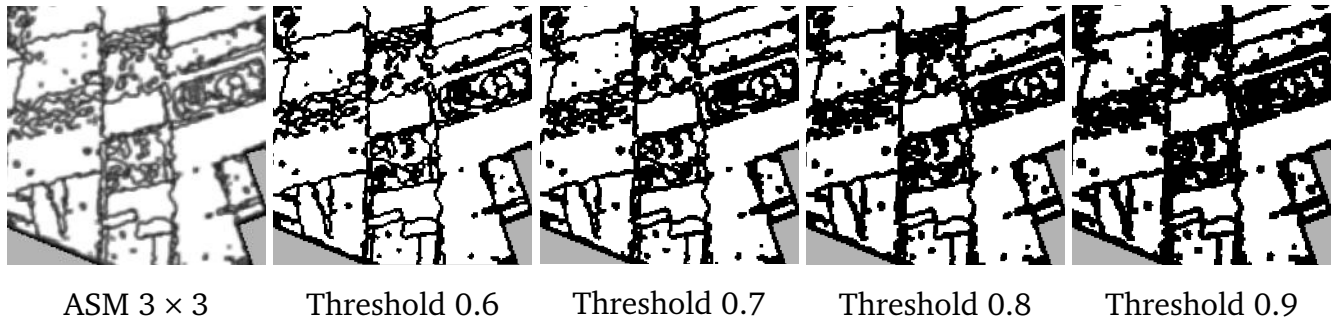


Figure 4.6.: Subset images with different thresholds around Fuhrberg. For raw classification see fig. 4.5.

Figure 4.6 provides an overview of the different thresholds. The higher the threshold (the closer to 1) the broader the lines and the thicker the field boundaries. In turn the inhomogeneous regions grew into one another.

Extensive, inhomogeneous fields were preferred to thin field limits. Associated therewith, it was decided for a threshold of 0.9 for the further procedure. Blackening the uncertainty map improved the visual appearance and delimited inhomogeneous surfaces.

4.3.2 Majority filter

The majority filter was tested to eliminate field borders from being part of the uncertainty. A filter with a broad window size was applied so that more bright pixels were captured inside the window that would dominate and remove the field borders from the uncertainty map. Here, a 5×5 majority filter was superimposed. The filter removed fine lines including field borders (see green circles in fig. 4.7), but reduced the extent of inhomogeneous areas (see red circles). Recall that tessellated areas indicate areas that are not part of the predefined classes. The objective is not only to find few pixels with uncertainties next to each other but a whole field. In the case of figure 4.7, the problem could have arisen because there were too many different dark grey levels so that white pixels obtained the majority.

The next step was to apply the majority filter on the binary version of the ASM-texture map. The width of the field boundaries stayed the same, but the counters were smoothed (fig. 4.8).

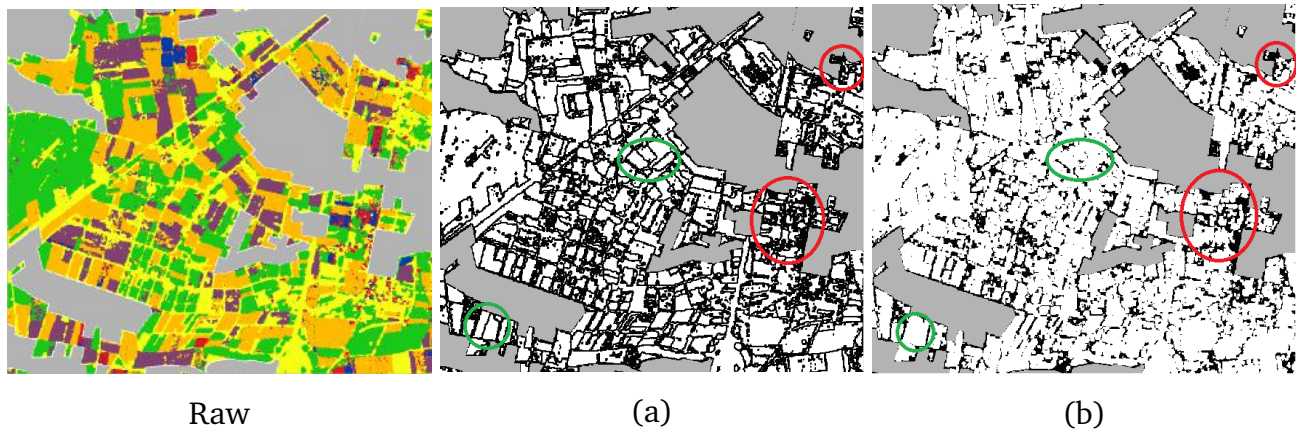


Figure 4.7.: Comparison of a majority filter with the initial texture analysis in a subset region around Celle. Green areas showed the desired effect, while red areas aggravated the result. (a) A 3×3 ASM, then binary values with threshold 0.9. (b) A 3×3 ASM, on it a majority filter 5×5 , then binary values with threshold 0.9. Values > 0.9 stand for a high certainty, while values < 0.9 stand for a low certainty.

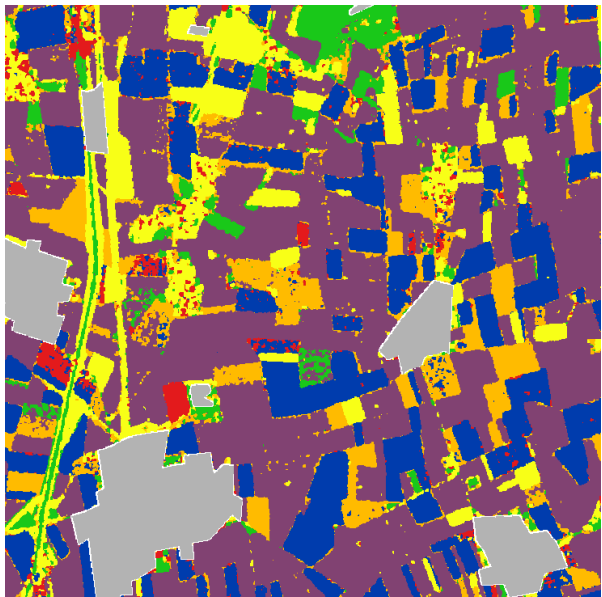
Moreover, the inhomogeneous surfaces were filled steadily with increasing iterations (see blue circles in fig. 4.8). Small irregularities within homogeneous surfaces were diminished (see blue circles in fig. 4.8).

To compare the results with a finer filter, a 3×3 majority filter was applied to the same map. The result was iterated four times because the small window size appeared only with small alterations after each repetition. The results showed that there was not much difference between the uncertainty map of a window size 3 or 5 (see fig. 4.9 for comparison). Nonetheless, the majority filter of 3×3 was preferred because it did not fill small homogeneous fields as much (see fig. 4.10).

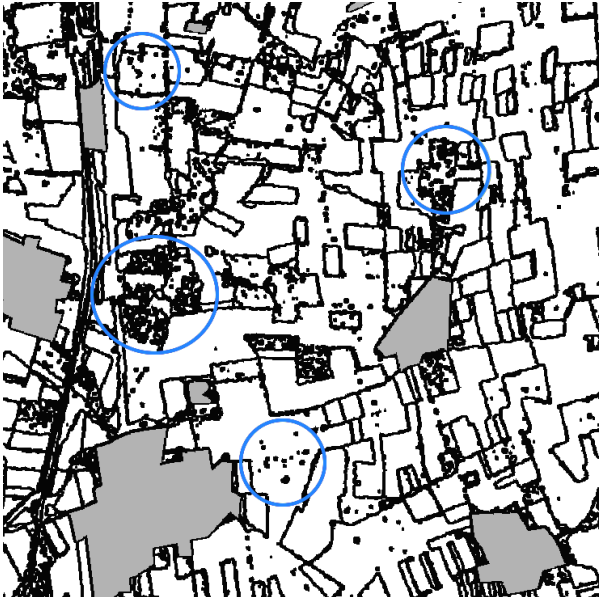
In summary, the texture analysis markedly improved the existing classification. The 0.9-binary- 3×3 -ASM texture achieved the best result. The majority filter added smaller improvements thereon. For example, it filled more of the inhomogeneous areas, it smoothed edges and deleted some isolated black pixels. Here, the 4 times iterated 3×3 majority filter was chosen as the best result. It can be found as a map in the Annex (see figure A.1).

4.4 Developed land-cover maps

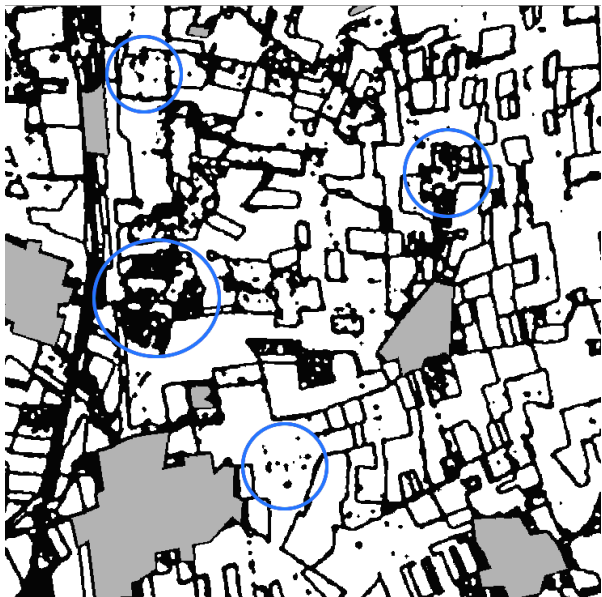
The best uncertainty maps were chosen to establish a user-friendlier map. For this purpose, the uncertainty map was merged with the raw classification from the starting situation. This was realised with an element-wise multiplication (see the code in Annex B.3). For an area of high certainty (value = 1) the original class was kept, whereas for an area of high uncertainty (value = 0) a new class "unclassified" was introduced (with a value of 0).



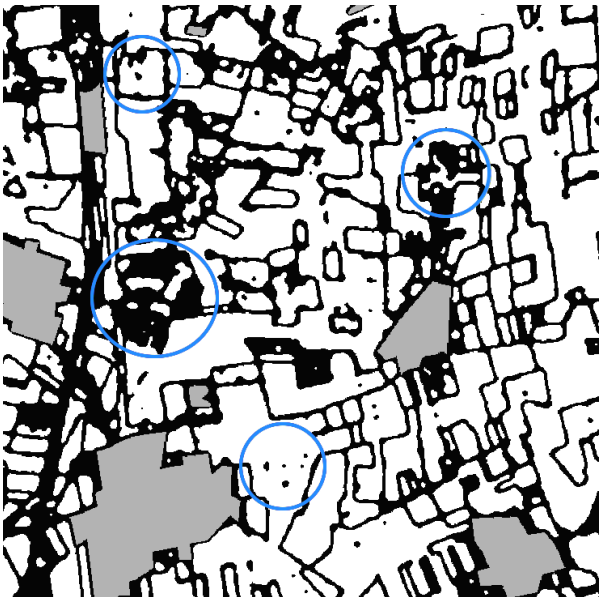
Raw classification



Binary ASM 3×3



Majority 5×5 , Iteration 0



Majority 5×5 , Iteration 2

Figure 4.8.: 5×5 Majority filter applied on a binary 3×3 ASM with a threshold of 0.9. Subset region of Algermissen.



Figure 4.9.: 3×3 majority filter after 4 iterations on a binary 3×3 ASM (threshold 0.9). Subset region of Algermissen.



Raw



Majority 3×3 (4 iterations)



Majority 5×5

Figure 4.10.: Comparison of majority filters in a subset region around Algermissen.

The land-cover maps for a binary 3×3 ASM and for an additional 3×3 majority filter applied on the binary 3×3 ASM can be found in the annex (see fig. A.3 and fig. A.4, respectively).

4.4.1 Visual comparison

While in the raw classification the patterns of different classes had been prominent, the new classifications pointed the viewer's eye towards the agricultural, homogeneous areas (fig. 4.11). At this time, isolated pixels of other classes as well as whole fields with patterns of different classes were blackened. The ASM texture revealed more areas of the old classification. It had a rather pixelated appearance. The majority filter, by contrast, smoothed the classification. Most tessellated areas turned black.

4.4.2 Statistical comparison

Figure 4.12 provides the summary statistics of how the newly created land-cover map changed the extent of the cultivation areas for the plant types of this investigation. In general, in the study area, grain was the main cultivation. Potato acres were rather rare. The size of the land halved for all type of uses except for grain in the course of post-processing. This observation indicates that the grain class itself had a high producer's accuracy because the field was rarely confused with another class of the classification. Similarly, the grain class had a high user's

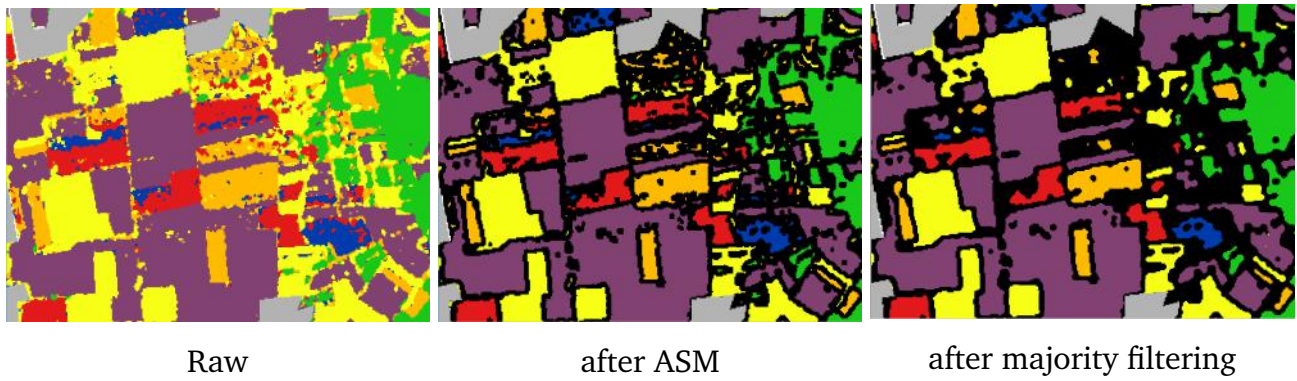


Figure 4.11.: Comparison of the original and the developed land cover maps. Black areas are areas of high uncertainty and were excluded from the classification result. Subset region around Neustadt am Rübenberge.

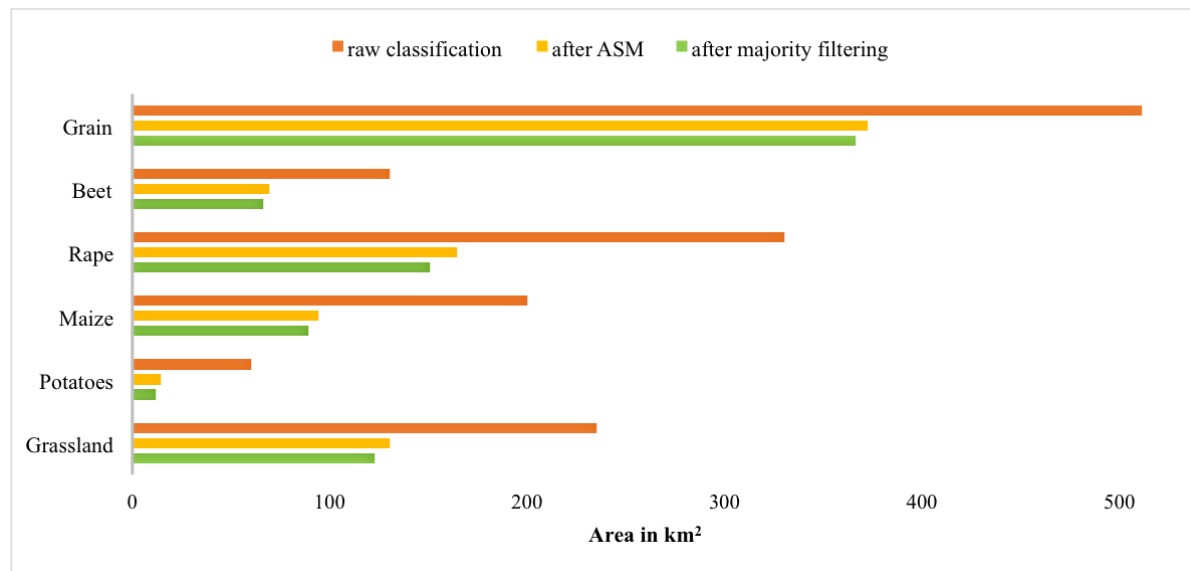


Figure 4.12.: Area of the respective class in the corresponding classification.

accuracy because the class was rarely chosen to be uncertain². Moreover, grain fields were often cultivated next to each other, so that no area was deleted because of field borders.

By contrast, oilseed rape and grassland lost a large portion of their former region because they were detected in many inhomogeneous areas, which revealed low accuracy. The amount of potato fields decreased because they often were confused with beet fields (cf. section 5.3).

The majority filter ameliorated the map proportionally slightly on a large scale, even though it filled many white holes in the small scale. Additional 34 km^2 out of $1,467 \text{ km}^2$ were shifted to "uncertain" (cf. table 4.1). The preceding 3×3 ASM calculation detected 621 km^2 of uncertain areas, which corresponds to 42 % of previously agricultural land.

² A high user's accuracy means that what is stated as grain in the map is highly probable to be grain on the ground.

4.5 Samples

The potential of the created map was investigated in the final part of the result section. For that reason, uncertain areas in the map were selected on a random basis. The respective land covers were captured with a camera equipped with a Global Positioning System (GPS). The map revealed areas with agricultural uses that were not part of the defined classes as well as areas with no agricultural usage.

One must note that the data for the classification were collected in 2015. Since not all field-covers were recorded at that time, some of the following pictures were taken in 2016. Consequently, the land use may have changed. For perennial crops it can be assumed that the product grown has not changed.

4.5.1 Unknown agricultural land covers

As mentioned in the introduction, not all agricultural land covers usually are included in the training data set. The essential reason for that is the dimension of the region to be classified. It is not possible to have data on every crop grown in that area. This is especially true for species that do not occur frequently.

Through random samples and non-matching fields that have been found during the field survey, the developed textures were checked for their veracity. Within the borders of the project area, black surfaces in the uncertainty maps were found out to be asparagus, onions, strawberries and "semi-natural" areas such as bee meadows. This means, areas that were found to have different land covers than the ones in the classification model, veritably were fully coloured black in the uncertainty map after the majority filter (meaning they had a high uncertainty).

An overview of the different species is listed below.

Asparagus (fig. 4.13) is a perennial plant with different development stages and appearance throughout the years, which makes it difficult to be detected by the classifier. The picture was taken one year after the classification, however it is reasonable to assume that the area had the same vegetation the previous year.

Onions (fig. 4.14) and strawberries (fig. 4.15) were subject to strong variations too.

Wild meadows were not classified in the original classification either. For example, a bee meadow with its beehives (fig. 4.16) was detected. On a different field, ruderal species were found (fig. 4.17). They normally occur when the field is no longer cultivated.

It was very interesting to find an abandoned beet field (fig. 4.18). The weed ranked so high that the beet was almost invisible. This changed the backscatter and the perception of the field. As it seemed not to be used any longer, it was correctly detected as uncertain.

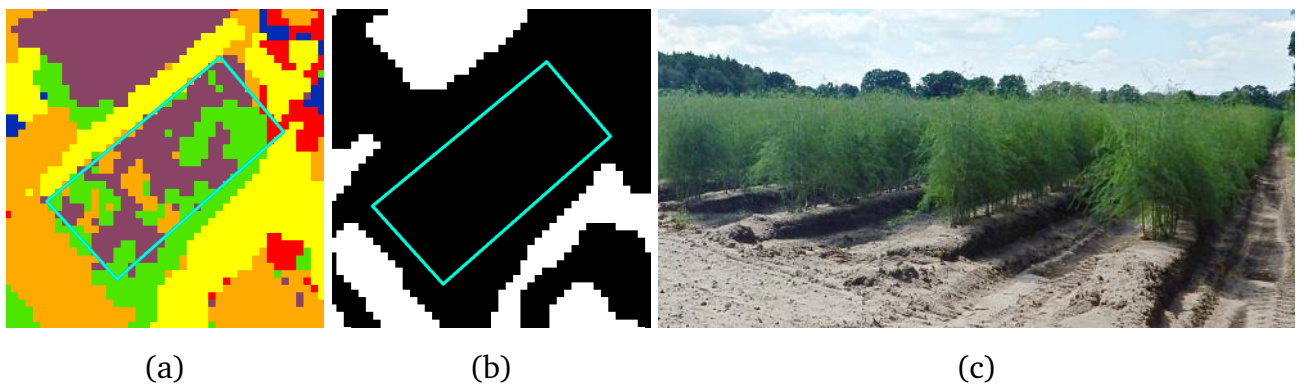


Figure 4.13.: Unknown agricultural class: asparagus. (a) Raw classification. (b) Uncertainty map after majority filtering. (c) GPS picture of the field taken on 27-06-2016.

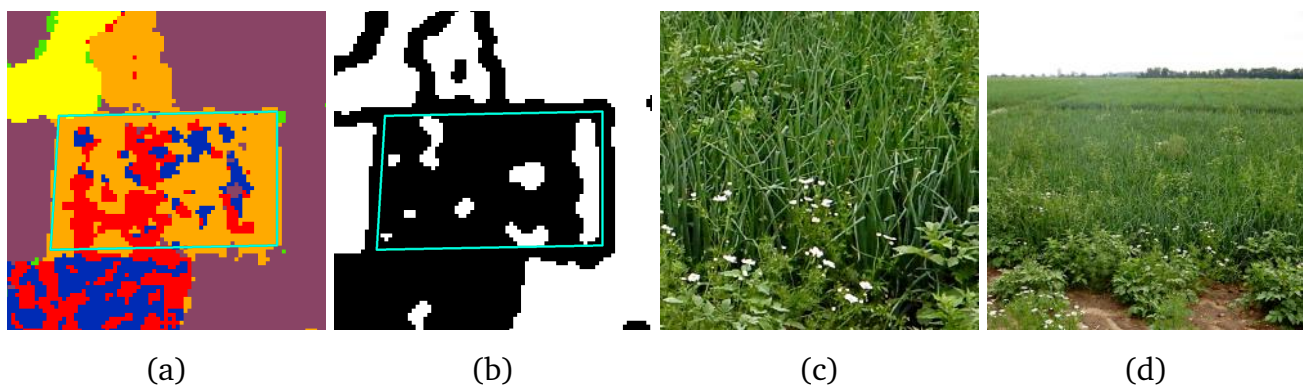


Figure 4.14.: Unknown agricultural class: onions. (a) Raw classification. (b) Uncertainty map after majority filtering. (c)-(d) GPS picture of the field taken on 22-07-2015.

Another example demonstrates an unexpected and sudden change in the agricultural use. Here, bare soil was detected by means of the uncertainty map that could point to ploughing up of grassland (fig. 4.19). The verification was carried out with satellite images from Google Earth, which covered the spring, summer and autumn of 2015. In doing so, no plant cover had been detected (see fig. 4.19c - e).

4.5.2 Non-agricultural land covers

Aside from lacking agricultural land covers, there were also non-agricultural land covers that were highlighted by the texture analysis. These included barren land, settlements and industrial territory.

As an example, an industrial territory was found that recycled building rubble (fig. 4.20). This indicates that not all land uses were entered in ATKIS.



Figure 4.15.: Unknown agricultural class: strawberries. (a) Raw classification. (b) Uncertainty map after majority filtering. (c) Aerial photo of the field taken from Google Earth on 01-07-2015 where people pick strawberries. (d) GPS picture of the field taken on 26-06-2016.

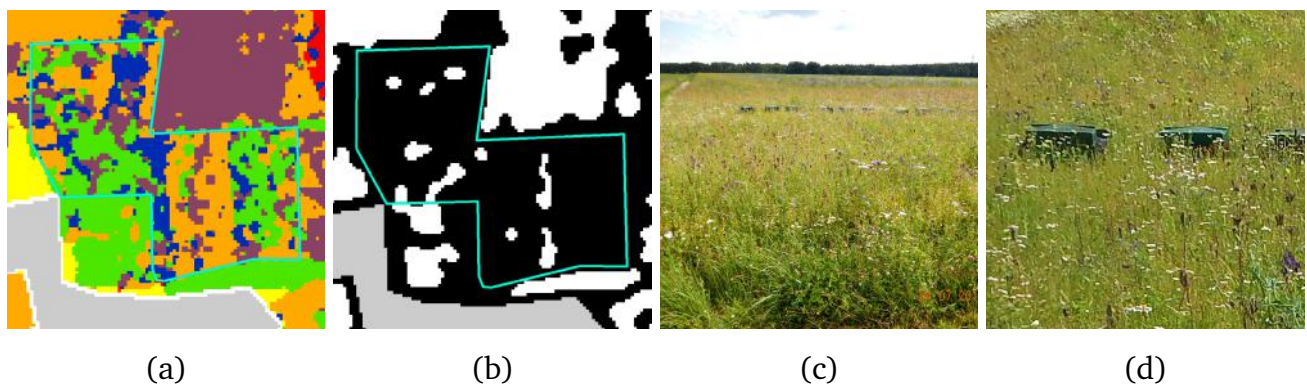


Figure 4.16.: Unknown agricultural class: bee pasture. (a) Raw classification. (b) Uncertainty map after majority filtering. (c)-(d) GPS pictures with beehives taken on 04-07-2016.

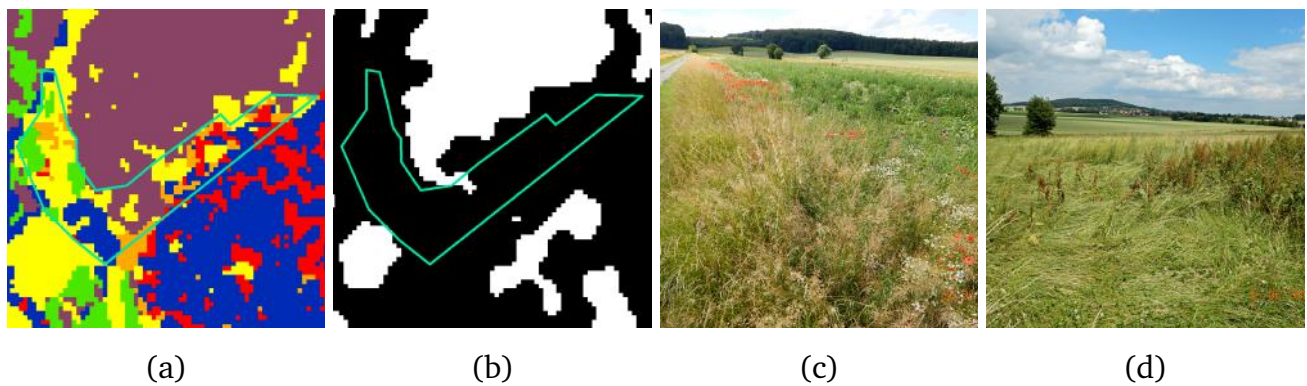


Figure 4.17.: Unknown agricultural class: ruderal species. (a) Raw classification. (b) Uncertainty map after majority filtering. (c)-(d) GPS pictures of the field taken on 26-07-2016.

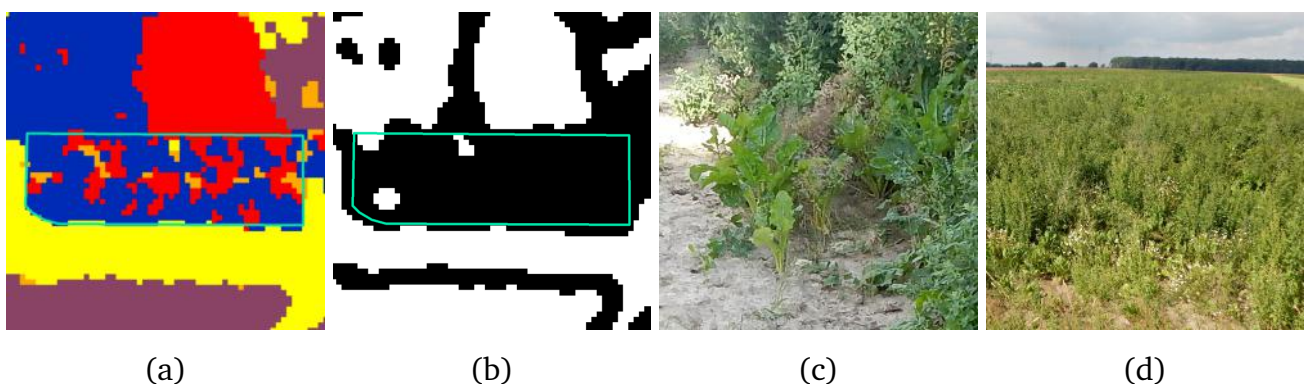


Figure 4.18.: Unrecognised class: weedy beet. (a) Raw classification. (b) Uncertainty map after majority filtering. (c)-(d) GPS pictures of the field taken on 23-07-2015.

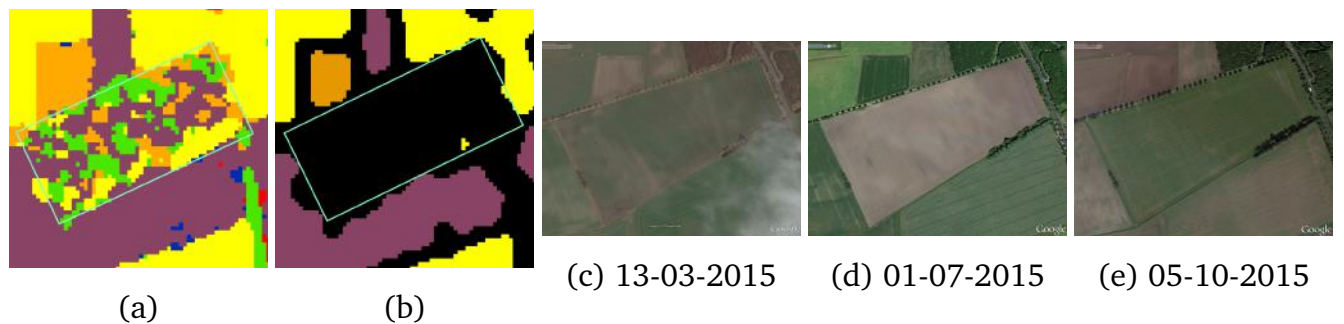


Figure 4.19.: Sudden change: possible ploughing up of grassland. (a) Raw classification. (b) Uncertainty map after majority filtering. (c)-(e) Aerial photos by Google Earth taken during the vegetation period 2015.

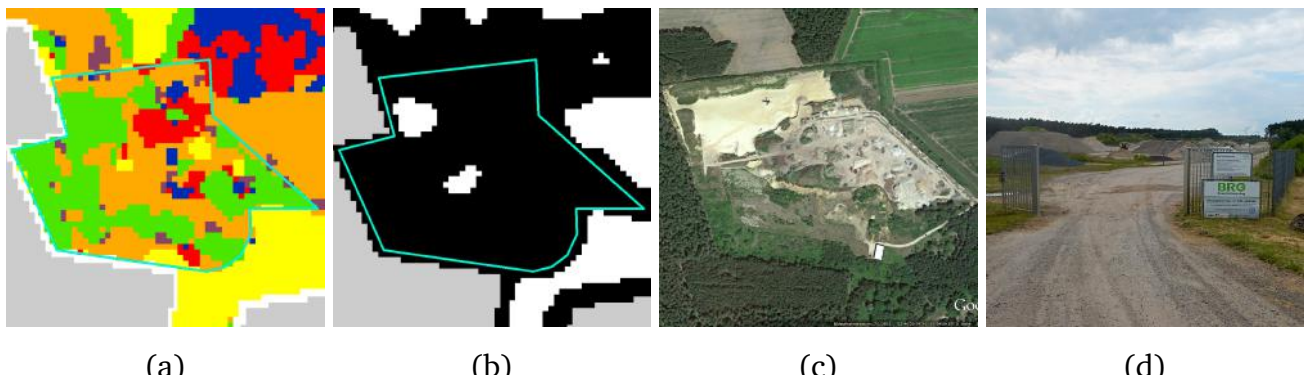


Figure 4.20.: Non-agricultural land: recycling of building rubble. (a) Raw classification. (b) Uncertainty map after majority filtering. (c) Aerial photo by Google Earth taken on 01-07-2015. (d) GPS picture of the field taken on 04-07-2016.

5 Discussion

5.1 Critical review

Our study has shown that assigning a rate of certainty to the class allocation noticeably enhances the classification results. Wrongly classified pixels are masked accordingly and thus prevented from entering into maps or statistics. This gives the map a higher degree of accuracy. The more a user will find the type of land use listed in the map on the ground, the higher is the accuracy of the map.

The most important finding that emerges from the analysis is that many land covers were found which were not represented within the set of class labels. This is particularly because, first, they represent a minority; second, their spectral information might be complex to interpret; or third, their vegetation-time perhaps lasted shorter than the inclusion period. Especially in agriculture, the cultivated plants change rapidly over time. It is not always possible to stay up-to-date with the current land covers when repeating the classification for another period of time, so that some classes or land covers might be missing in other years.

For this reason, the classification was improved substantially by moving uncertain pixels to a new class "unclassified". While the number of pixels of the classified agricultural products decreased, the internal statistics (the ratio of the products) changed. A positive aspect is that as a result, the completeness of the map increases, because it opens the possibility of other classes being present as well.

The findings remind that even though the classification accuracy is high, it must not reflect the exact situation on-site. The accuracies described in section 2.4 are always just a measure to compare how well the classifier is able to recognise the sample areas (the reference data), meaning places that are known to contain one of the classes. [30, p. 100] There is no guarantee that other areas, which are not part of the reference data and to which a particular class is assigned, really contain that class. Our study therefore provides a tool to locate areas that have a high probability to contain a land cover that does not exist in the classification model.

Moreover, CPP was sensitive to irregularities within fields that belong to the predetermined classes. As an example, a field was marked as uncertain because the shafts of the grain were broken by the wind.

Finding only irregularities that were relevant to the problem definition has only been possible by combining classes with similar spectral information (e.g. different cereal species were merged into grain). Otherwise, there would have been many more uncertain regions that would have been detected because of a bad accuracy of the classes themselves. This would however not lead

to an enhanced classification result. In fact, through the method suggested in this investigation, more completeness is added to the map because it is based on the assumption that there are more classes than the predefined classes on the ground.

Our results are based on the assumption that the classification delivers high-quality results. The more accurate the classifier is, the closer to reality the results of the texture analysis are, because there will no longer be misclassified pixels within the field borders of one of the predetermined classes. This means all the black areas in the final land-cover map stand for unknown land covers.

The knowledge of uncertain areas in the land cover map is an important information for users (authorities, scientists, etc.). Otherwise, users would conclude that only six (or thirteen) different crops are grown in the area. Furthermore, the accumulations of different classes inside a small radius will confuse users or make them sceptical about the correctness of the map. The developed land-cover maps only pass on information that has a high probability of being correct. The agricultural land visible in the map was extracted by deleting all other land covers, such as waters, forests and settlements. For this, ATKIS served as an information base, which is kept up to date by the Land Surveying Office. However, the uncertainty map revealed that some non-agricultural areas have not been entered into the topographic map (or data base) yet. For example due to urbanisation, cities grow quickly and new development areas are initiated. They are however not immediately registered in the ATKIS data base (see fig. 5.1). The co-occurrence analysis thus was helpful to identify those places. This result is very encouraging especially with regard to countries whose geographic-basic-data are not as advanced as the German equivalent ATKIS.



(a)



(b)

Figure 5.1.: Development area in Celle. (a) Final land cover map after majority filter. (b) Picture by Google Earth taken on 01-07-2015.

5.2 Comparisons to previous studies and application

Research articles about CPP generally place emphasis on the refinement of class labels (filtering, MRF, relearning; cf. [25]), which means a reallocation of the existing classes. This approach is preceded by the assumption that the map only reflects what the class labels represent. Howe-

ver, seeing that the arable lands have strong temporal and spatial dynamics, the conventional methods do not seem suitable for the agricultural sector. In reviewing the literature, no recommendations were found on how to enhance the classification results in agriculture. Therefore, we suggest to use our approach, which enables the consideration of new classes.

The approach to use the class labels' co-occurrence has mainly been applied to classification pre-processing and was only recently introduced to CPP by Huang et al. [25]. Whereas the authors at the time focused to improve the accuracy of the individual classes by reallocation, this study set out with the aim of assessing an enhancement through the knowledge of uncertainties, which only indirectly improves the accuracy of the single classes. Overall, it upgrades the classification by reducing the number of misclassified pixels.

Moreover, authorities (such as state offices or the European Union) highlight the need for satellite-based classifications. Among others the State Office of Lower Saxony shares the vision to automate the main survey of land use. Areas of the same land uses can be added up and harvest statistics can be derived. All this pre-supposes that the crop types can be differentiated from one another. [26] The Julius-Kühn-Institute further points out the advantage of a timely availability of remote sensing data that supports a quick evaluation and a quicker knowledge about the security of supply to the population. Hitherto, nationwide statistics are published one-and-a-half or two years after harvest. The institute envisages a web portal for yield prognosis that is launched during the simultaneous vegetation season. [29]

5.3 Limitations and errors



Rail tracks and street close to Luedersen.



Field paths and trees close to Springe.

Figure 5.2.: Different forms of plot borders in the study area. Pictures by Google Earth taken on 01-07-2015.

Plot borders do not necessarily represent an uncertainty but an effect that occurs because two different land covers are situated next to each other. It was not possible to eliminate plot borders and to completely fill inhomogeneous regions at the same time. Map creators have to set their priorities beforehand. Large uncertain (i.e. black) areas entail thick plot borders, whereby the latter result in an over-abundance of uncertain pixels. By contrast, non-existing plot borders

entail errors in the inhomogeneous regions that remain undetected. Both decisions influence the statistics of classification products to a greater or lesser extent. However, weeds, shrubs and tracks regularly line the margins of the fields (fig. 5.2). The Chamber of Agriculture of Lower Saxony advises to maintain this ecotone¹ [27]. These observations imply that margins of the field may be factored in the uncertain surfaces.

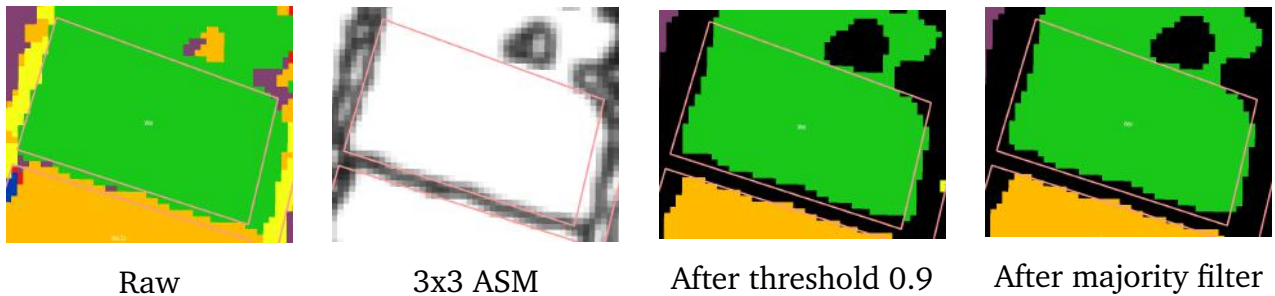


Figure 5.3.: Before-and-after: How plot borders run into the beet field. Field close to Wietze.

The plot borders filled some of the space of the homogeneous areas (fig. 5.3). This effect arose through the 3×3 moving window during the texture calculation and was increased by setting a threshold value. This means that some correct (certain) pixels were erroneously excluded from the map and thus reduce the occurrence of the existing classes in the statistics wrongly.

The recognition of homogeneous fields depends on their width. The possible interference of two plot borders in close proximity, especially in conjunction with a majority filter, cannot be ruled out. In addition, small fields could have been mistaken for an irregular spot. As a result, the field can disappear if it is too narrow (see fig. 5.4). The width of such narrow fields corresponds to a maximum of a few hundred meters. Thereby, the respective areas are far less than a square kilometre and negligible with regard to the size of the project area (cf. the classes' sum in table 4.1 on page 42).

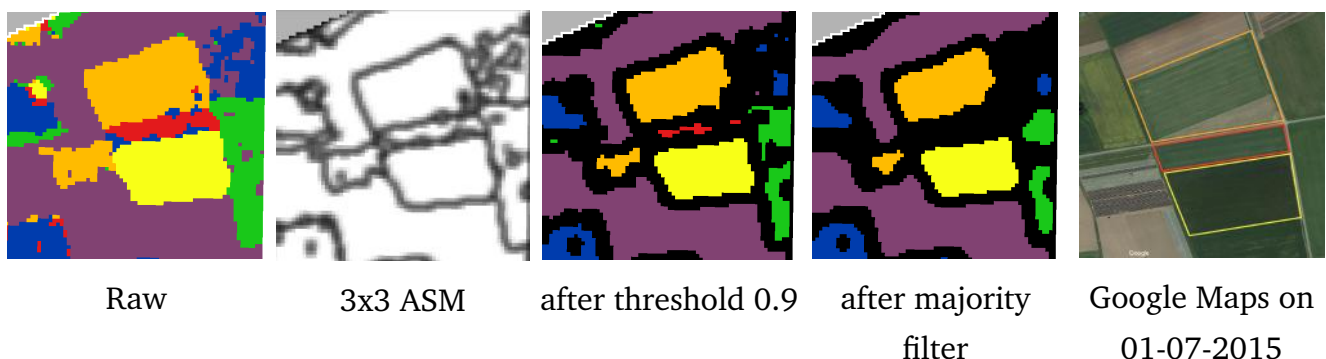


Figure 5.4.: How small areas disappear through post-processing. Subset region around Burgdorf.

¹ The term "ecotone" refers to grassy margin strips or shrubs between two fields, which make a positive contribution to the biodiversity.

Even though many fields were deleted which were not part of the predefined classes, there are still wrong areas that stayed undetected. For areas to be found, they need to consist of patches of different classes. If the region is mistaken e.g. for oilseed rape instead (rape, because it has a low user's accuracy), the homogeneity within the field stays high and the uncertainty low. As a consequence, they are still visible in the revised map. This happened in particular in the case of forests and settlements (see fig. 5.5). In the bigger picture this means that classes with a low user's accuracy will also evince a low but improved user's accuracy after the rearrangement.

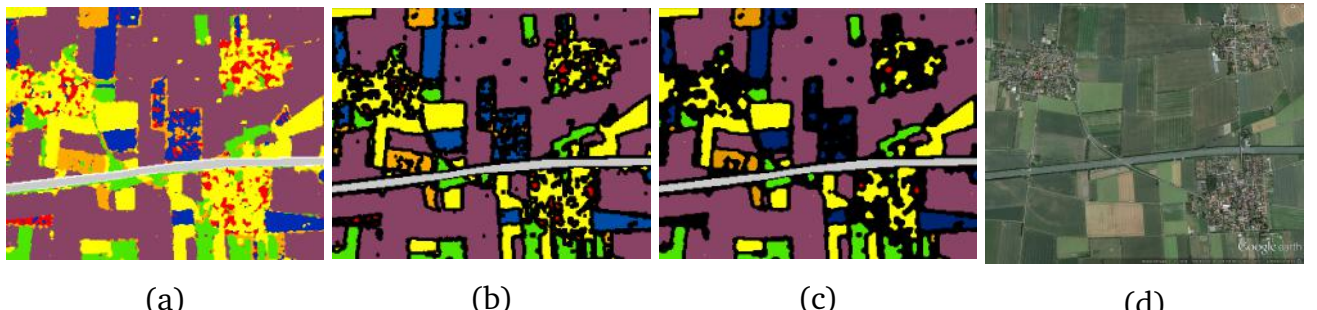


Figure 5.5.: Undetected settlements with a relatively high occurrence of oilseed rape. (a) Raw classification. (b) Final land-cover map after ASM. (c) Final land-cover map after majority filter. (d) Picture with settlements by Google Earth taken on 01-07-2015.

We must add that both potatoes and beets in some cases are confused with one another in the classification. Thus both land covers showed a high rate of uncertainty and were blackened. This means the occurrence of both is wrongfully too low in the statistics (cf. fig. 4.12).

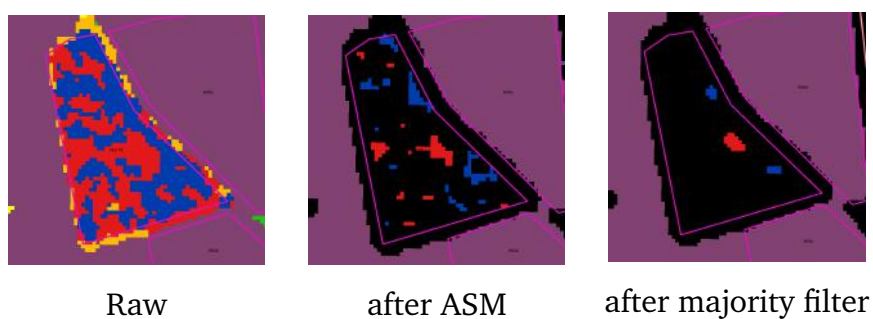


Figure 5.6.: Training sample of a beet field with high occurrence of potatoes.



6 Conclusion and outlook

6.1 Conclusion

The purpose of the current study was to investigate the possibilities to upgrade the classification results of an agricultural area through CPP. We showed that the conventional methods are not versatile enough to adopt to considerable spatial and temporal fluctuations as prevailing in agriculture. The relevance of our approach is clearly supported by the various fields we located whose land-covers differed from the classes in the classification model (e.g. farmland with unclassified crops or vegetation-free areas). One of the more significant findings to emerge from this study is that 42% to 45% of the farmland in the project area was subject to uncertainty. This is revealing because this high uncertainty level occurred even though the respective accuracies of the classes were very high. In general, therefore, it seems reasonable to accept that accuracies themselves cannot always provide information on how correct a map is in reality.

The results of this investigation show that the internal statistics of cultivation areas substantially improved by reducing the number of faulty pixels. Only pixels with a high certainty with regard to their class allocation entered the final land-cover map. This resulted in a higher accuracy. By adding a new class that is representative for all uncategorised land-covers, the map is further given a higher correctness and completeness, because it leaves room for new land-covers. Apart from this, applying a majority filter smoothens the result.

The generalisability of these results is subject to certain limitations. For instance, the co-occurrence analysis only leads to useful results, if the classifier can distinguish between the predefined classes. Moreover, the analysis was over-sensitive to field borders. In general, our approach has proved useful when not all classes in the set of class labels are known and in addition may be irrelevant to know for the question of the study.

6.2 Recommendations for further research work

Despite these promising results, an unconsidered factor are the errors that occur due to the broad plot borders, which protrude in fields and cause narrow fields to disappear. Future trials should assess to which extent broad plot borders negatively influence the proportion of uncertain areas. To minimise the error, the study should be repeated using different filters or CPP methods to evaluate the possibilities to diminish the plot borders and at the same time to expand the line structures in broader inhomogeneous regions. Subsequently, we propose to try

region growing, a technique for image segmentation. The aim should be to remove individual black spots within the plot borders of homogeneous fields by expanding the class of the homogeneous area. Furthermore, it would be interesting to know if there are options to distinguish uncertain surfaces and assign them to subcategories, e.g. "built-up areas" and "other agriculturally used areas".

Several fields that were known to be asparagus were attested by a high rate of uncertainty, because there was no own class assigned to it. Further research should be undertaken to investigate how asparagus fields or other perennial crops can be detected by a classifier in the first place.

A continuation of this work is to improve the accuracy of oilseed rape, which often occurred in areas of other land covers but was not detected as incorrect. For a classifier, oilseed rape is especially difficult to distinguish from shrubs. One possible solution is to examine oilseed rape individually, i.e. only the areas that have been classified as such. To this end, a time of the year is regarded in which the oilseed rape has a unique characteristic, e.g. during rape blossom (see fig. 6.1). While the areas will bloom yellow in the multi-spectral range in any case, the rapeseed areas will also appear as a defined signal in radar images. At the time of a unique characteristic, one to three radar images are chosen and compared to areas that pretend to be oilseed rape. If they present the characteristic, they are kept; otherwise, the area will be blackened and moved to the class "unclassified".



Figure 6.1.: A rapeseed field end of April in the Hannover region.

6.3 Applicability

This research, in accordance with Huang et al. [25, p. 7140], proves to be particularly valuable to demonstrate how CPP has the potential to enhance the classification results in more than only improving the classification accuracy and should serve as a base for future studies. Henceforth, the findings recommend a role for scientists in promoting CPP, which has often been neglected so far.

The methods used for agricultural areas in Hannover can be applied to other agricultural areas elsewhere in the world. In general, the research has several practical applications. Firstly, it can verify the data set in ATKIS. As an example, we suggest to use it to review if the real plot borders

(the one appearing in the map) comply with the registered entries in the database. Furthermore, the map indicates where unauthorised constructions might have taken place.

Secondly, the information gained from this study can be used to verify organic farming. It was shown that the co-occurrence analysis ranked weed in fields as an uncertainty (see 4.18), as weed reflects a different amount of backscatter. Organic farming does not use chemical substances and hence weed reproduces in the fields. This means, weed or irregularities have to be detected in the fields where farmers claim to grow organically. Normally an authorised person from the state has to go on-site, which costs time and money. Through remote sensing this job can be done way faster and with less effort and fewer resources. The rate of uncertainty in the particular fields is calculated and provides information on the cultivation method.



List of Cited Literature

- [1] W. L. Adamowicz, H. R. Akçakaya, A. Arcenas, S. Babu, D. Balk, U. Confalonieri, W. Cramer, F. Falconí, S. Fritz, R. Green, E. Gutiérrez-Espeleta, K. Hamilton, R. Kane, J. Latham, E. Matthews, T. Ricketts, and T.X. Yue. *Analytical Approaches for Assessing Ecosystem Condition and Human Well-being*. In: *Ecosystems and Human Well-being: Current State and Trends, Volume 1*, chapter 2, pages 37–71. Island Press, 2005.
- [2] F. Albrechtsen. Statistical texture measures computed from gray level cooccurrence matrices. Nov 2008.
- [3] Arbeitsgemeinschaft der Vermessungsverwaltungen der Länder der Bundesrepublik Deutschland (AdV). Amtliches Topographisch-Kartographisches Informationssystem (at-kis). <http://www.adv-online.de/AAA-Modell/ATKIS/>, n.d. [Online; accessed 27-July-2016].
- [4] D. Bargiel. *Klassifikation von Agrarflächen auf Basis von hoch aufgelösten Radarbildern des Satelliten TerraSAR-X als Grundlage zur räumlichen Abbildung von Ökosystemdienstleistungen*. PhD thesis, Gottfried Wilhelm Leibniz Universität Hannover, 2013.
- [5] T. Blaschke. Object based image analysis for remote sensing. *ISPRS Journal of Photogrammetry and Remote Sensing*, 65(1):2–16, Jan 2010.
- [6] A. C. Bovik. *The Essential Guide to Image Processing*. Academic Press, 2nd edition, Jul 2009.
- [7] J. Cohen. A coefficient of agreement for nominal scales. *Educational and Psychological Measurement*, 20(1):37–46, 1960. doi: 10.1177/001316446002000104.
- [8] R. G. Congalton. A review of assessing the accuracy of classifications of remotely sensed data. *Remote Sensing of Environment*, 37(1):35–46, Jul 1991. doi: 10.1016/0034-4257(91)90048-B.
- [9] R. G. Congalton. Thematic and positional accuracy assessment of digital remotely sensed data. In *Proceedings of the Seventh Annual Forest Inventory and Analysis Symposium*, Gen. Tech. Report WO-77, pages 149–154. United States Department of Agriculture, Oct 2005.
- [10] R. G. Congalton and K. Green. *Assessing the accuracy of remotely sensed data : principles and practices*. Mapping science series. CRC Press, Taylor & Francis Group, Boca Raton, 2nd edition, 2009.

- [11] Copernicus. Application domains in agriculture, forestry and fisheries. <http://www.copernicus.eu/main/agriculture-forestry-and-fisheries>, n.d. [Online; accessed 27-May-2016].
- [12] EEA (European Environment Agency). Assessing biodiversity in europe — the 2010 report. EEA Report 5, Kongens Nytorv 6, 1050 Copenhagen K, Denmark, 2010.
- [13] EPA (United States Environmental Protection Agency). Climate impacts on agriculture and food supply. <https://www3.epa.gov/climatechange/impacts/agriculture.html#area>, n.d. [Online; accessed 28-June-2016].
- [14] ESA Earth Online. Sentinel-1 : Mission details. <https://earth.esa.int/web/guest/missions/esa-operational-eo-missions/sentinel-1>, n.d. [Online; accessed 27-May-2016].
- [15] Eurostat : Statistics Explained. Lucas - land use and land cover survey. http://ec.europa.eu/eurostat/statistics-explained/index.php/LUCAS_-_Land_use_and_land_cover_survey, n.d. [Online; accessed 26-July-2016].
- [16] FAO (Food and Agriculture Organization of the United Nations). How to manage biodiversity for food and agriculture. <http://www.fao.org/agriculture/crops/thematic-sitemap/theme/spi/scpi-home/managing-ecosystems/biodiversity-and-ecosystem-services/bio-how/en/>, n.d. [Online; accessed 27-May-2016].
- [17] M. Fauvel, J. Chanussot, and J. A. Benediktsson. A spatial-spectral kernel based approach for the classification of remote sensing images. *Pattern Recognition*, 45(1):381–392, Jan 2012.
- [18] C. Gardi, L. Montanarella, D. Arrouays, A. Bispo, P. Lemanceau, C. Jolivet, C. Mulder, L. Ranjard, J. Römbke, M. Rutgers, and C. Menta. Soil biodiversity monitoring in europe: ongoing activities and challenges. *European Journal of Soil Science*, 60(5):807–819, 2009. doi: 10.1111/j.1365-2389.2009.01177.x.
- [19] S. Geman and D. Geman. Stochastic relaxation, gibbs distributions, and the bayesian restoration of images. *IEEE Transactions on Pattern Analysis and Machine Intelligence*, PAMI-6(6):721–741, Nov 1984. ISSN 0162-8828. doi: 10.1109/TPAMI.1984.4767596.
- [20] Google Inc. Google earth. <https://www.google.de/intl/de/earth/>, May 2015. [Online; accessed 8-Aug-2016].

- [21] R. M. Haralick, K. Shanmugam, and I. Dinstein. Textural features for image classification. *IEEE Transactions on Systems, Man, and Cybernetics*, SMC-3(6):610–621, Nov 1973. doi: 10.1109/TSMC.1973.4309314.
- [22] High Level Expert Forum. Global agriculture towards 2050. In *How to feed the world in 2050*, Rome, Oct 2009. FAO (Food and Agriculture Organization of the United Nations).
- [23] R. J. Hijmans. *Geographic Data Analysis and Modeling*, 2.5-2 edition, Dec 2015. [Online; accessed 21-April-2016].
- [24] W. Hollweg and U. Kollek. Ernte 2015: Erträge besser als anfangs befürchtet. <https://www.lwk-niedersachsen.de/index.cfm/portal/7/nav/1095/article/28191.html>, Oct 2015.
- [25] X. Huang, Q. Lu, L. Zhang, and A. Plaza. New postprocessing methods for remote sensing image classification: A systematic study. *IEEE Transactions on Geoscience and Remote Sensing*, 52(11):7140–7159, Nov 2014. doi: 10.1109/TGRS.2014.2308192.
- [26] G. Keckl. Die ermittlung der amtlichen Hektarerträge für Feldfrüchte in Niedersachsen und Ernteergebnisse 2001 : Flächenerkundung über Satellit. Niedersächsisches Landesamt für Statistik (NLS) via http://www.nls.niedersachsen.de/Tabellen/Landwirtschaft/bee_text/e_stat.htm, 2001. [Online; accessed 26-July-2016].
- [27] N. Kretzschmar. Hinweise zur Pflege von Randstreifen. Landwirtschaftskammer Niedersachsen via <https://www.lwk-niedersachsen.de/index.cfm/portal/betriebumwelt/nav/199/article/22158.html>, Jul 2015. [Online; accessed 13-July-2016].
- [28] J. R. Landis and G. G. Koch. The measurement of observer agreement for categorical data. *Biometrics*, 33(1):159–174, 1977.
- [29] H. Lilienthal and H. Gerighausen. Regionale fernerkundliche Erfassung des aktuellen landwirtschaftlichen Ertragspotenzials. Julis Kühn-Institut via http://www.d-copernicus.de/sites/default/files/dokumente/Forum_2014/Vortrag_Gerighausen.pdf, Apr 2014. [Online; accessed 26-July-2016].
- [30] J. G. Liu and P. J. Mason. *Image Classification*. In: *Essential Image Processing and GIS for Remote Sensing*, chapter 8, pages 91–103. John Wiley & Sons, Inc., 2009. doi: 10.1002/9781118687963.ch8.
- [31] P. M. Mather and M. Koch. *Computer Processing of Remotely-Sensed Images: An Introduction*. John Wiley & Sons, Ltd, 4th edition, 2010.

- [32] D. K. McIver and M. A. Friedl. Using prior probabilities in decision-tree classification of remotely sensed data. *Remote Sensing of Environment*, 81(2/3):253–261, Aug 2002.
- [33] S. W. Myint, N. S.-N. Lam, and J. M. Tyler. Wavelets for urban spatial feature discrimination: Comparisons with fractal, spatial autocorrelation, and spatial co-occurrence approaches. *Photogrammetric Engineering & Remote Sensing*, 70(7):803–812, Jul 2004.
- [34] Natural Resources Canada. Polarization in radar systems. <http://www.nrcan.gc.ca/earth-sciences/geomatics/satellite-imagery-air-photos/satellite-imagery-products/educational-resources/9567>. [Online; accessed 25-July-2016].
- [35] Niedersächsisches Ministerium für Ernährung, Landwirtschaft und Verbraucherschutz. Ergänzungen zur Broschüre : Die niedersächsische Landwirtschaft in Zahlen 2014, Jul 2016.
- [36] F. Pacifici, M. Chini, and W. Emery. A neural network approach using multiscale textural metrics from very high-resolution panchromatic imagery for urban land-use classification. *Remote Sensing of Environment*, 113(6):1276–1292, Jun 2009.
- [37] M. Pal and P. M. Mather. An assessment of the effectiveness of decision tree methods for land cover classification. *Remote Sensing of Environment*, 86(4):554–565, Aug 2003.
- [38] E. Pebesma and R. Bivand. *Classes and Methods for Spatial Data*, 1.2-3 edition, Apr 2014. URL <https://cran.r-project.org/web/packages/sp/sp.pdf>. [Online; accessed 8-Aug-2016].
- [39] J.S. Rawata and M. Kumarb. Monitoring land use/cover change using remote sensing and gis techniques: A case study of hawalbagh block, district almora, uttarakhand, india. *The Egyptian Journal of Remote Sensing and Space Science*, 18:77–84, Jun 2015. URL <http://www.sciencedirect.com/science/article/pii/S1110982315000034>.
- [40] J. A. Richards. *Remote Sensing with Imaging Radar*. Signals and Communication Technology. Springer-Verlag Berlin Heidelberg, 1st edition, 2009.
- [41] F. Schmidt. Geosetter. <http://www.geosetter.de/>, Feb 2011. [Online; accessed 8-Aug-2016].
- [42] A. Schubert, D. Small, N. Miranda, D. Geudtner, and E. Meier. Sentinel-1A product geolocation accuracy: Commissioning phase results. *Remote Sensing*, 7:9431–9449, Jul 2015.
- [43] B. Solaiman, R. K. Koffi, M. C. Mouchot, and A. Hillion. An information fusion method for multispectral image classification postprocessing. *IEEE Transactions on Geoscience and Remote Sensing*, 36(2):395–406, Mar 1998. ISSN 0196-2892. doi: 10.1109/36.662725.

-
- [44] J. Stuckens, P. R. Coppin, and M. E. Bauer. Integrating contextual information with per-pixel classification for improved land cover classification. *Remote Sensing of Environment*, 71(3):282–296, Mar 2000.
 - [45] C. Tomasi and R. Manduchi. Bilateral filtering for gray and color images. In *Proceedings of the 1998 IEEE International Conference on Computer Vision*, pages 839–846, Bombay, India, 1998.
 - [46] R. Tortora. A note on sample size estimation for multinomial populations. *The American Statistician*, 32(3):100–102, Aug 1978.
 - [47] A. Vance. Data analysts captivated by r’s power. http://www.nytimes.com/2009/01/07/technology/business-computing/07program.html?_r=0, Jan 2009. [Online; accessed 6-June-2016].
 - [48] A. Zvoleff. *Calculate Textures from Grey-Level Co-Occurrence Matrices (GLCMs)*, 1.6.1 edition, Mar 2016. [Online; accessed 1- June-2016].



A Maps

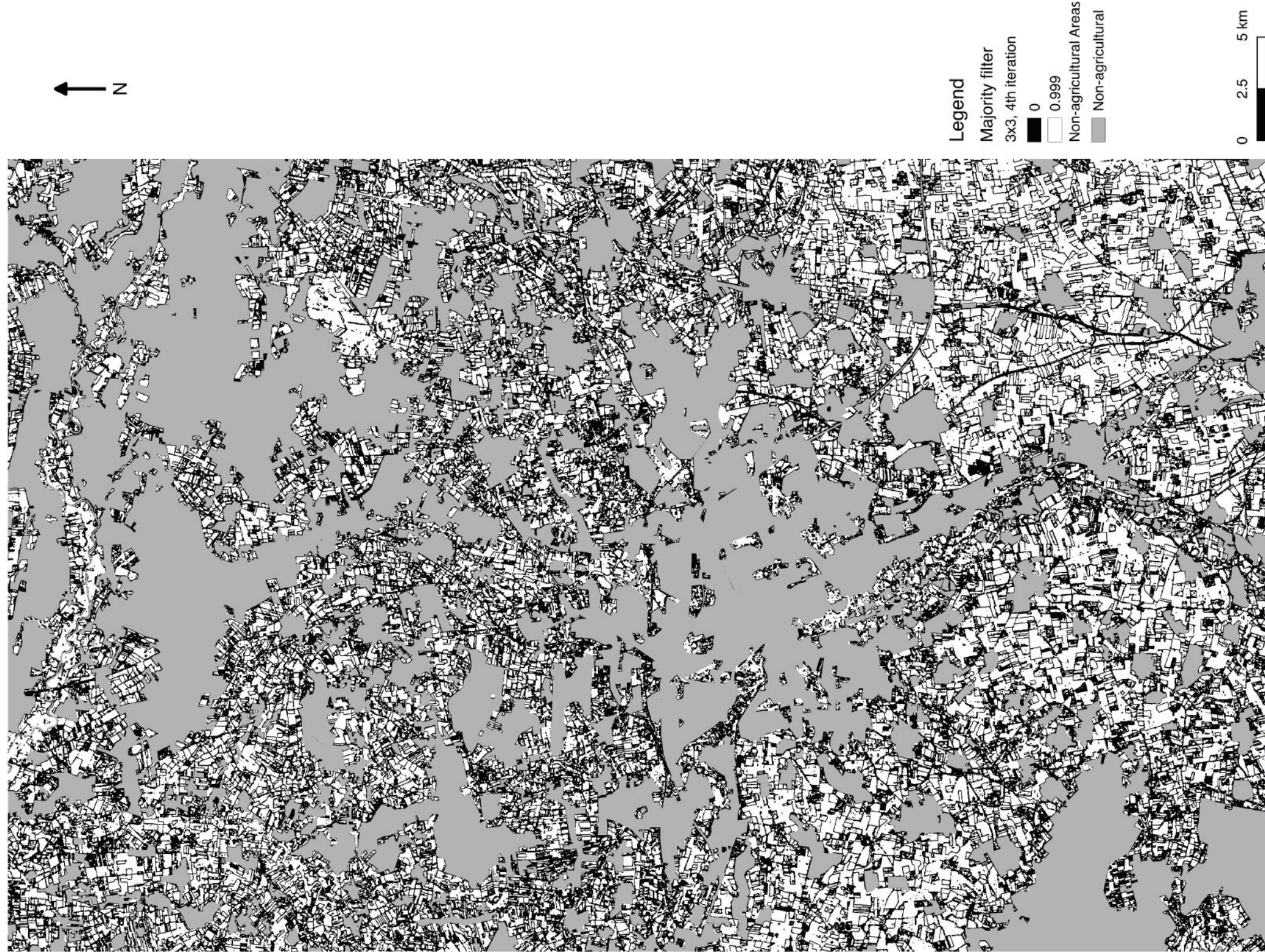


Figure A.1.: 3×3 ASM Texture with a 3×3 majority filter on top. A value of 0 indicates a high uncertainty, while a value around 1 indicates a high homogeneity.

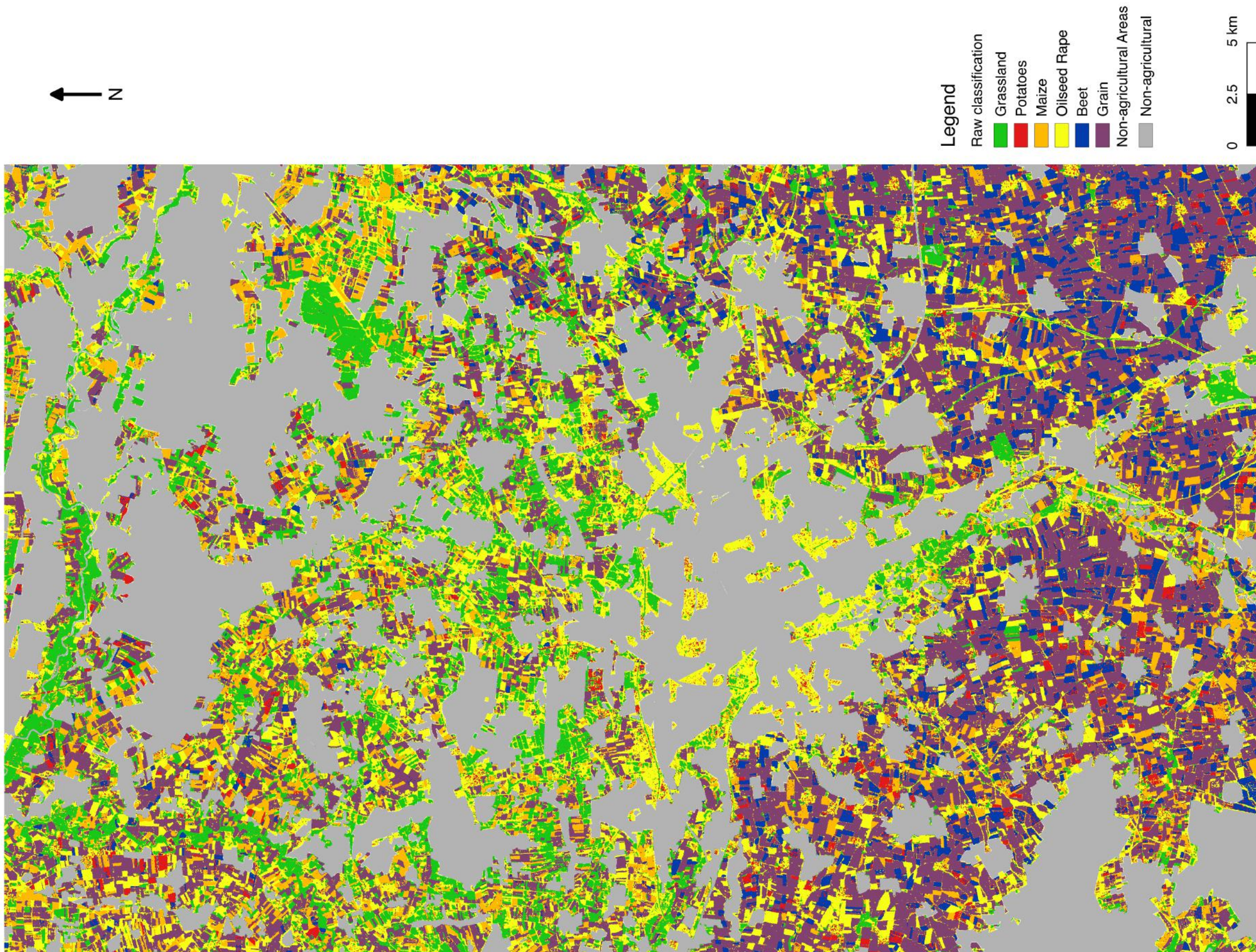


Figure A.2.: Raw land-cover map. The 13 original classes have been reduced to 6.

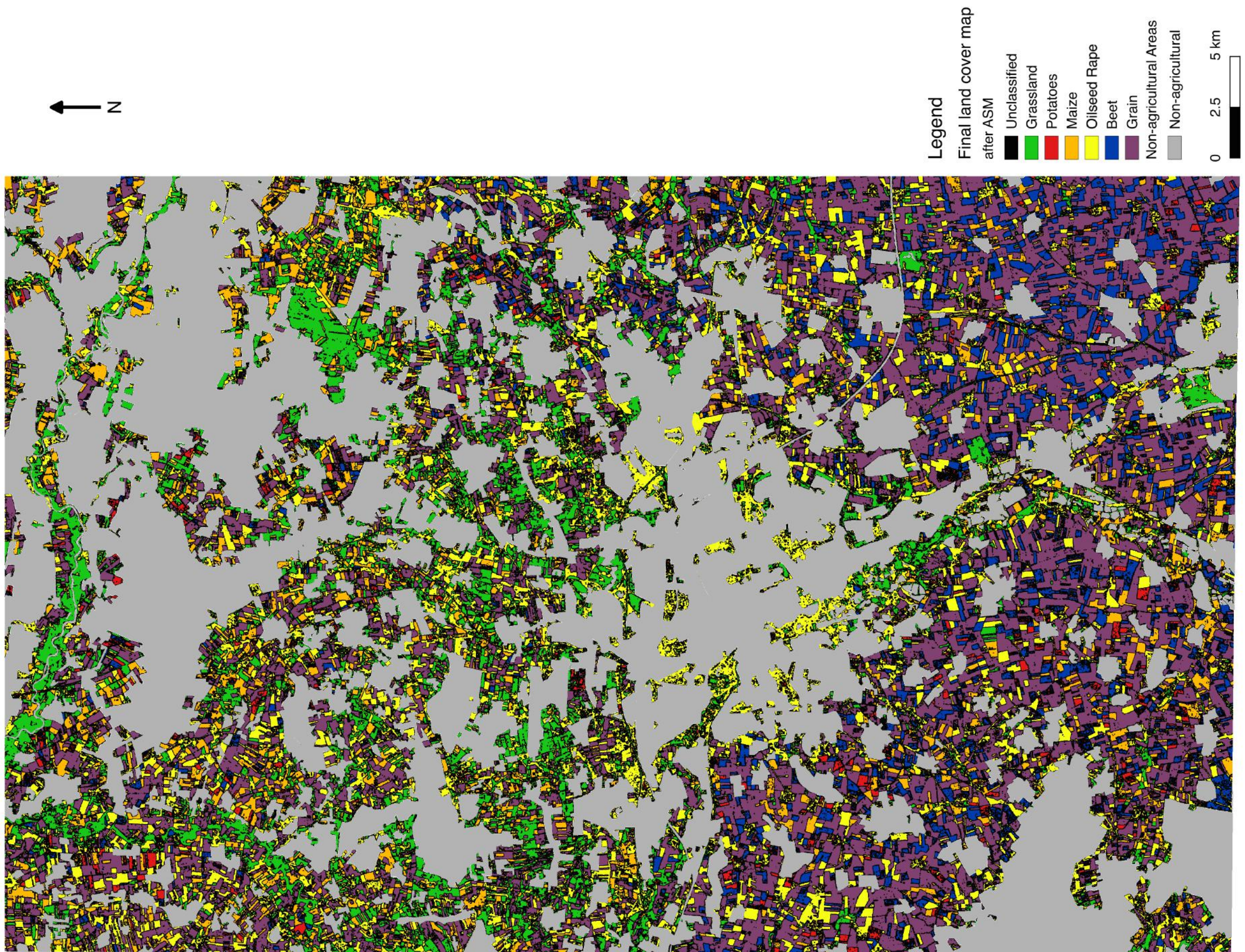


Figure A.3.: Final land-cover map. Created from a 3×3 ASM with a threshold of 0.9.

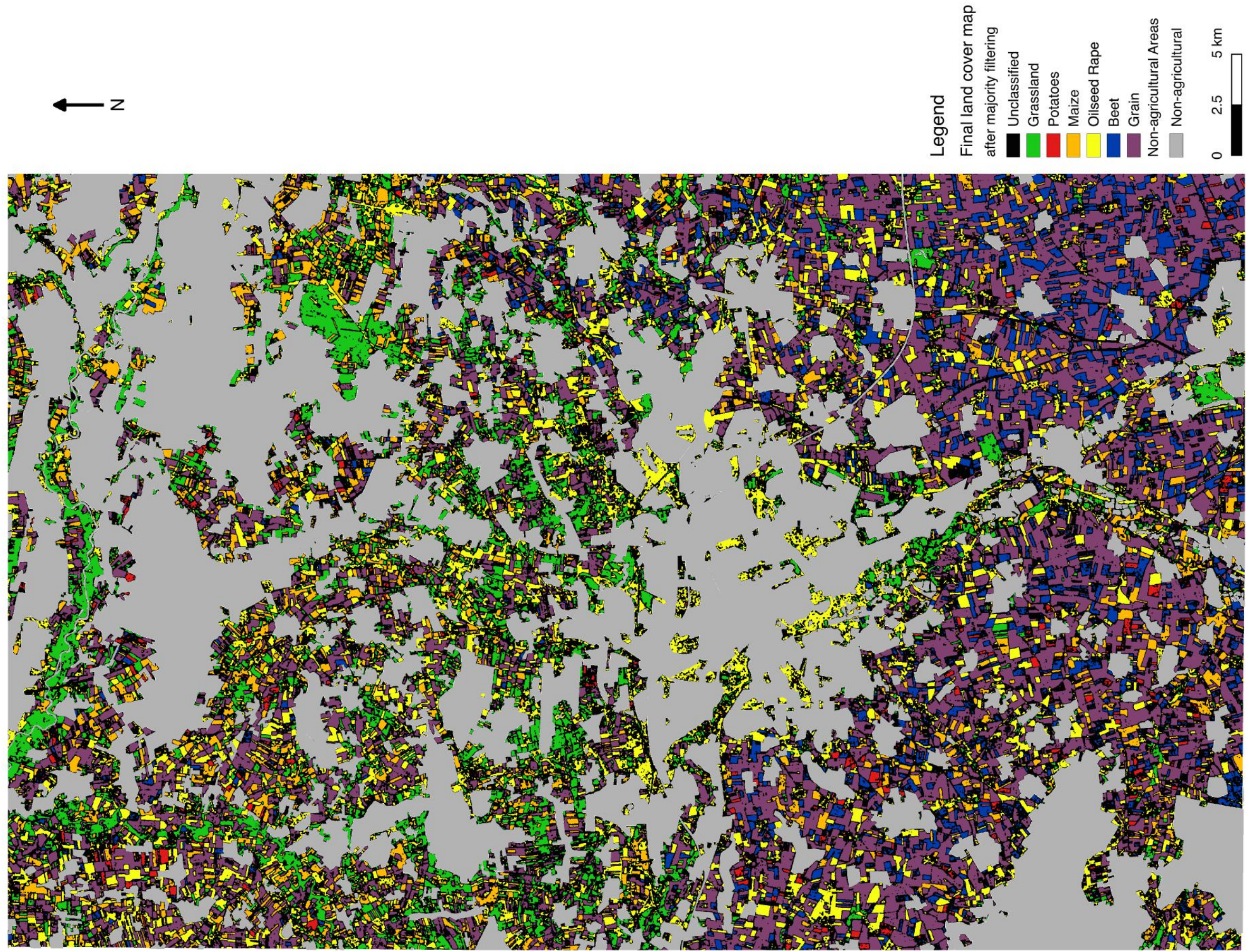


Figure A.4.: Final land-cover map. Created from a four times iterated 3×3 majority filter on a 3×3 ASM with a threshold of 0.9.

B Code

All code sections start with loading the same packages:

```
# Calling packages
library("sp")
library("raster")
library("rgdal")
library("maptools")
library("lattice")
library("tcltk")
library("glcm")
```

B.1 Texture analysis

```
# Reading in the data and creating a RasterLayer object
raw_classification <- raster(file.choose())

# _____ TEXTURE ANALYSIS _____ #

# Vector for different window sizes
window <- c(3,5,7,9)

# Textural features used in the analysis
text_features <- c("variance", "homogeneity", "entropy", "second_moment")

# directions: shifts of 0, 45, 90 and 135 degrees
direction <- list(c(0,1), c(1,1), c(1,0), c(1,-1))

# Calculating the GLCMs

for (w in window) {
```

```

stacks <- glcm(raw_classification, n_grey = 13, window = c(w, w), shift = direction,
                statistics = text_features, na_opt="ignore", na_val=NA, scale_factor=1,
                asinteger=FALSE)
# na_opt here: NA values will be ignored
# the 4 different textural features are saved in different layers of the stack

if (w==3) {
  variance_3 <- stacks[[1]]
  homogeneity_3 <- stacks[[2]]
  entropy_3 <- stacks[[3]]
  second_moment_3 <- stacks[[4]]
} else if (w==5) {
  variance_5 <- stacks[[1]]
  homogeneity_5 <- stacks[[2]]
  entropy_5 <- stacks[[3]]
  second_moment_5 <- stacks[[4]]
} else if (w==7) {
  variance_7 <- stacks[[1]]
  homogeneity_7 <- stacks[[2]]
  entropy_7 <- stacks[[3]]
  second_moment_7 <- stacks[[4]]
} else if (w==9) {
  variance_9 <- stacks[[1]]
  homogeneity_9 <- stacks[[2]]
  entropy_9 <- stacks[[3]]
  second_moment_9 <- stacks[[4]]
}
}

# Writing of the new textures
writeRaster(variance_3, 'D:\\\\Analyse\\\\variance_3x3.tif')
writeRaster(variance_5, 'D:\\\\Analyse\\\\variance_5x5.tif')
writeRaster(variance_7, 'D:\\\\Analyse\\\\variance_7x7.tif')
writeRaster(variance_9, 'D:\\\\Analyse\\\\variance_9x9.tif')

writeRaster(homogeneity_3, 'D:\\\\Analyse\\\\homogeneity_3x3.tif')

```

```

writeRaster(homogeneity_5, 'D:\\Analyse\\homogeneity_5x5.tif')
writeRaster(homogeneity_7, 'D:\\Analyse\\homogeneity_7x7.tif')
writeRaster(homogeneity_9, 'D:\\Analyse\\homogeneity_9x9.tif')

writeRaster(entropy_3, 'D:\\Analyse\\entropy_3x3.tif')
writeRaster(entropy_5, 'D:\\Analyse\\entropy_5x5.tif')
writeRaster(entropy_7, 'D:\\Analyse\\entropy_7x7.tif')
writeRaster(entropy_9, 'D:\\Analyse\\entropy_9x9.tif')

writeRaster(second_moment_3, 'D:\\Analyse\\asm_3x3.tif')
writeRaster(second_moment_5, 'D:\\Analyse\\asm_5x5.tif')
writeRaster(second_moment_7, 'D:\\Analyse\\asm_7x7.tif')
writeRaster(second_moment_9, 'D:\\Analyse\\asm_9x9.tif')

# _____ ITERATION OF ASM _____ #

# Window size: 3x3
w <- 3

# Textural feature
text_features <- "second_moment"

# Directions : shifts of 0, 45, 90, and 135 degrees
direction <- list(c(0,1), c(1,1), c(1,0), c(1,-1))

# ____ Calculating the GLCMs for an ASM texture

# ____ Iteration 0
asm_from_asm <- glcm(raw_classification, n_grey = 9, window = c(w, w), shift =
  direction, statistics = text_features, na_opt="ignore", na_val=NA, scale_factor=1,
  asinteger=FALSE)
#n_grey set to 9 because there are values from 1 to 9 in the classification

writeRaster(asn_from_asm, 'D:\\Analyse\\asn_from_asm_iter0_raw.tif')

```

```
# ____ Iteration 1 to 5: homogeneity texture applied to the previous homogeneity texture
# ____ then assigns the result to variable which includes the number of the iteration

for (i in 1:5) {

  asm_from_asm <- glcm(asm_from_asm, n_grey = 13, window = c(w, w), shift =
    direction, statistics = text_features, na_opt="ignore", na_val=NA, scale_factor=1,
    asinteger=FALSE)

  writeRaster(asm_from_asm,
    paste("D:\\\\Analyse\\\\asm_from_asm_iter",i,"_raw.tif",sep=""))
}
```

B.2 Smoothing the result

B.2.1 Setting a threshold

```
# Reading in the 3x3 ASM texture (not iterated)
asm_3x3_raw <- raster(file.choose())

# Setting a threshold, here 0.9
threshold <- matrix(c(0, 0.9, 0, 0.9, 1, 1), ncol=3, byrow=TRUE)
  #if there are overlapping ranges, the first time a number is within a range determines
  #the reclassification value

# Reassign values
asm_from_asm_iter0_raw_binary <- reclassify(asym_3x3_raw, threshold)

writeRaster(asym_from_asm_iter1_raw_binary,
  "D:\\\\Analyse\\\\asm_from_asm_iter0_raw_binary_ts09.tif")
```

B.2.2 Applying a majority filter

The majority filter has been applied with the "focal" function of the "raster" package, which implements a moving window. Therein the function "modal" has been used, which reports the most frequent value of sample results.

```
# Reading in the ASM texture with the uncertainties
asm <- raster(file.choose())
asm_binary <- raster(file.choose()) # binary with threshold 0.9

# _____ Window size: 5x5
window = matrix(1,nrow = 5,ncol = 5)

# Majority filter on the grey-scale texture
asm_majority <- focal(asym, w=window, fun=modal)
writeRaster(asym_majority, 'D:\\\\Analyse\\\\asm_3x3_majority_5x5.tif')

# Majority filter on the binary texture
asm_majority <- focal(asym_binary, w=window, fun=modal)
writeRaster(asym_majority, 'D:\\\\Analyse\\\\asm_3x3_bin_ts90_majority_5x5.tif')

# _____ Window size: 3x3
window = matrix(1,nrow = 3,ncol = 3)

# Majority filter on the grey-scale texture
asm_majority <- focal(asym, w=window, fun=modal)
writeRaster(asym_majority, 'D:\\\\Analyse\\\\asm_3x3_majority_3x3.tif')

# Majority filter on the binary texture
asm_majority <- focal(asym_binary, w=window, fun=modal)
writeRaster(asym_majority, 'D:\\\\Analyse\\\\asm_3x3_bin_ts90_majority_3x3.tif')

# _____ Window size: 3x3, iterated, binary
```

```

window = matrix(1,nrow = 3,ncol = 3)

# Majority filter on the binary texture, zeroth iteration
asm_bin_majority <- focal(asm_binary, w=window, fun=modal)

# Majority filter on the previous texture map, iteration 1 to 4
for (i in 1:4) {
  asm_bin_majority <- focal(asm_bin_majority, w=window, fun=modal)
}

writeRaster(asm_bin_majority,
  'D:\\Analyse\\majority_3x3_iter4_from_asm_3x3_bin_ts90.tif')

```

B.3 Area calculation

The raw classification as stated in section 3.1 had class numbers (or values) from 1 to 9. Based on the binary uncertainty map it was decided for every pixel whether its class identity is kept or not. A zero means the class was probably wrongly classified and should be deleted from the map; a one means it was probably correct and should be kept. By multiplying every pixel in the raw classification by the value in the binary uncertainty map, all pixels with the value zero were eliminated from the classification.

Afterwards, the number of pixels that remained in each class could be counted separately with the function "freq" of the "raster" package.

```

# Reading in the data
raw_classification <- raster(file.choose())      # Initial classification , 6 classes
asm_3x3_bin_90 <- raster(file.choose())          #Angular Second Moment, 3x3 window,
binary version (threshold 0.9)
asm_3x3_majority <- raster(file.choose())        #Majority filter of the Angular Second
Moment, 3x3 window, binary version (threshold 0.9)

```

```
# _____ MATRIX MULTIPLICATION _____ #
```

```

# Raw_classification has class numbers from 1 to 9. The uncertainty map indicates if the
class is kept or not (0=deleted, 1=kept)

```

```
# a*b: elementwise operation
certain_areas_asm <- raw_classification * asm_3x3_bin_90
certain_areas_majority_asm <- raw_classification * asm_3x3_majority

# Writing of the new maps
writeRaster(certain_areas_asm, 'D:\\\\Ergebnisse\\\\certain_area_asm_3x3_from_ts90.tif')
writeRaster(certain_areas_majority_asm,
'D:\\\\Ergebnisse\\\\certain_area_majority_3x3_from_asm_3x3_ts90.tif')

# _____ COUNTING AREAS _____ #

# Check the resolution
show(raw_classification)

# Frequency
# How often does each value in the classification occur?
freq(raw_classification)
freq(certain_areas_asm)
freq(certain_areas_majority_asm)
```



Eidesstattliche Erklärung

Erklärung zur Abschlussarbeit gemäß § 22 Abs. 7 APB der TU Darmstadt

Hiermit versichere ich, Korinna Schmitz, die vorliegende Bachelor-Thesis ohne Hilfe Dritter und nur mit den angegebenen Quellen und Hilfsmitteln angefertigt zu haben. Alle Stellen, die Quellen entnommen wurden, sind als solche kenntlich gemacht worden. Diese Arbeit hat in gleicher oder ähnlicher Form noch keiner Prüfungsbehörde vorgelegen.

In der abgegebenen Thesis stimmen die schriftliche und elektronische Fassung überein.

Darmstadt, den _____

Unterschrift